Palaeontology
The Palaeontological Association
Registered Charity No. 11683330

A NEW SMALL, MESOROSTRINE INIOID (CETACEA, ODONTOCETI, DELPHINIDA) FROM FOUR LATE MIOCENE LOCALITIES OF THE PISCO BASIN, PERU

Journal:	*Palaeontology*
Manuscript ID	PALA-03-20-4738-OA
Manuscript Type:	Original Article
Date Submitted by the Author:	25-Mar-2020
Complete List of Authors:	Lambert, Olivier; Institut royal des Sciences naturelles de Belgique, D.O. Terre et Histoire de la Vie Collareta, Alberto Benites-Palomino, Aldo Di Celma, Claudio de Muizon, Christian; Muséum National d'Histoire Naturelle, USM 0203 - UMR 5143 CNRS, Paléobiodiversité et paléoenvironnements Urbina, Mario; Museo de Historia Natural, Universidad Nacional Mayor de San Marcos, Departamento de Paleontologìa de Vertebrados Bianucci, Giovanni; Università di Pisa, Dipartimento di Scienze della Terra
Key words:	Inioidea, Pontoporiidae, dolphin, late Miocene, Tortonian, Pisco Formation

Note: The following files were submitted by the author for peer review, but cannot be converted to PDF. You must view these files (e.g. movies) online.

Lambert et al_suppl file1_character-taxon matrix.nex
Lambert et al_suppl file2_molecular constraint tree.nex

A NEW SMALL, MESOROSTRINE INIOID (CETACEA, ODONTOCETI, DELPHINIDA) FROM FOUR LATE MIOCENE LOCALITIES OF THE PISCO BASIN, PERU

OLIVIER LAMBERT*[,1], ALBERTO COLLARETA[2], ALDO BENITES-PALOMINO[3,4], CLAUDIO DI CELMA[5], CHRISTIAN DE MUIZON[6], MARIO URBINA[4] *and* GIOVANNI BIANUCCI[2]

[1]Direction Opérationnelle Terre et Histoire de la Vie, Institut Royal des Sciences Naturelles de Belgique, rue Vautier 29, 1000 Brussels, Belgium; email: olambert@naturalsciences.be

[2]Dipartimento di Scienze della Terra, Università di Pisa, Via S. Maria 53, 56126 Pisa, Italy

[3]Paläontologisches Institut und Museum, Universität Zürich, Karl-Schmid-Straße 4, 8006 Zürich, Switzerland

[4]Departamento de Paleontología de Vertebrados, Museo de Historia Natural – UNMSM, Avenida Arenales 1256, 15072 Lima, Peru

[5]Scuola di Scienze e Tecnologie, Università di Camerino, Via Gentile III da Varano 1, 62032 Camerino, Italy

[6]CR2P UMR 7207, (MNHN, CNRS, UPMC, Sorbonne-Université), Muséum national d'Histoire naturelle, Département Origines et Evolution, rue Cuvier 57, 75231 Paris, France

*Corresponding author

Abstract: The moderately rich past diversity of the superfamily Inioidea (Cetacea, Odontoceti) in both the Atlantic and Pacific oceans contrasts with the present survival of a

single genus (*Inia*, Amazon river dolphin, family Iniidae) in freshwater deposits of South America and of a single species (*Pontoporia blainvillei*, Franciscana, family Pontoporiidae) along the eastern coast of that continent. However, part of the late Miocene to Pliocene inioid fossil record is made of relatively fragmentarily known species, for which systematic affinities remain poorly understood. Based on a sample of six cranial specimens from early late Miocene (Tortonian, 9.5-8.6 Ma) marine deposits of the Pisco Formation in four localities of the East Pisco Basin (southern coast of Peru), we describe a new genus and species of inioid, *Samaydelphis chacaltanae*. Bearing a proportionally short rostrum with an upper tooth count of about 30 teeth per row, this small-sized species is characterized by a moderately elevated vertex of the cranium displaying a long anteromedial projection of the frontals and interparietal, as well as by the plesiomorphic retention of a premaxilla-nasal contact. Recovered as a member of the family Pontoporiidae in our phylogenetic analysis, *S. chacaltanae* falls as sister-group to *Meherrinia isoni*, from the late Miocene of North Carolina (U.S.A.), which has previously been tentatively referred to the Iniidae or regarded as a stem Inioidea. Originating from the P1 allomember of the Pisco Formation, the mesorostrine *S. chacaltanae* was contemporaneous and sympatric with two other inioids, the brevirostrine pontoporiid *Brachydelphis mazeasi* and the longirostrine iniid *Brujadelphis ankylorostris*.

Key words: Inioidea, Pontoporiidae, dolphin, late Miocene, Tortonian, Pisco Formation

INTRODUCTION

The two modern inioid (Cetacea, Odontoceti, Inioidea) genera, *Inia* (the Amazon river dolphin, the only extant member of the family Iniidae; Best & da Silva 1989) and *Pontoporia*

(the Franciscana, the only extant member of the family Pontoporiidae, from the coastal ecosystems along the eastern coast of South America; Brownell 1989), represent relics of a once much more diversified toothed cetacean clade (Cozzuol 2010; Marx *et al.* 2016). With a fossil record traced back to the late Miocene, extinct inioids have been recorded from numerous marine and, to a lesser extent, freshwater deposits across the world, testifying for a much broader past geographic distribution that spanned the north and southeast Atlantic as well as the northwestern and southeastern Pacific (Pyenson & Hoch 2007; Godfrey & Barnes 2008; Gibson & Geisler 2009; Geisler *et al.* 2012; Pyenson *et al.* 2015; Murakami 2016; Post *et al.* 2017; Lambert *et al.* 2018). The prevalence of extinct inioids in marine deposits and their broad geographic distribution have been brought as arguments in favour of the hypothesis of an ancestral habitat in marine environments for these small to medium-sized dolphins (Cassens *et al.* 2000; Hamilton *et al.* 2001; Geisler *et al.* 2011).

The past diversity of this clade in South America can be divided in two geographic and palaeoenvironmental domains: on the one hand, the freshwater deposits of Brazil and Argentina; on the other hand, the marine deposits along the Atlantic, Caribbean, and Pacific coasts of the continent (Muizon 1984, 1988*a*; Gutstein *et al.* 2009, 2014; Cozzuol 2010; Lambert & Muizon 2013; Aguirre-Fernández *et al.* 2017; Lambert *et al.* 2017). A vast majority of the late Miocene marine records originate from the East Pisco and Sacaco basins, located along the southern coast of Peru and famous for their extremely rich and increasingly well stratigraphically constrained marine mammal assemblages (e.g., Muizon 1984, 1988*a*; Bianucci *et al.* 2016*a, b*; Bosio *et al.* 2020*a, b*). Furthermore, the degree of completeness of inioid cranial remains from these two nearby regions contrasts markedly with fossil inioid material from other parts of the world. For example, finely preserved iniid and pontoporiid remains from the East Pisco Basin provided useful clues on the anatomy of cranial parts (e.g., the highly diagnostic ear bones) that are not preserved in closely related taxa from Central

America and the North Atlantic (Lambert & Muizon 2013; Lambert *et al.* 2017). Further exploiting this unique source of information on the early steps of the inioid evolutionary history, based on six new cranial specimens, mandible fragments, and a few associated vertebrae from early late Miocene deposits exposed at four localities of the East Pisco Basin, herein we describe a new inioid genus and species, and we investigate its phylogenetic relationships with other inioids worldwide.

GEOLOGICAL, STRATIGRAPHIC AND PALAEONTOLOGICAL FRAMEWORK

The East Pisco shelf basin in southern Peru is an extensional forearc basin elongated parallel to the Peruvian trench and is separated from the adjacent West Pisco upper-slope basin by a structural high (the Outer Shelf High), which is composed of Precambrian and Paleozoic metamorphic and igneous rocks (Thornburg and Kulm 1981; León *et al.* 2008). During much of its Cenozoic depositional history, the East Pisco Basin was a semi-enclosed, shallow-water, marine embayment protected seawards by a chain of basement islands (Marocco & Muizon 1988; Bianucci *et al.* 2018). Following rapid uplift during the latest Neogene (Pilger 1981; Hsu 1992; Macharé & Ortlieb 1992; Hampel *et al.* 2004), the basin fill became largely exposed in the present-day Ica Region, between the towns of Pisco and Nazca.

The sediments from which the fossil cetaceans described herein were collected are part of the middle to upper Miocene strata of the Pisco Formation exposed in the Ica desert. The Pisco Formation is the geologically youngest unit among those comprising the sedimentary fill of the East Pisco Basin (Dunbar *et al.* 1990; DeVries 1998), and consists of shallow-marine and offshore deposits – including gravels, sandstones, diatomaceous siltstones, nodular dolomitic beds, and tephra layers – that are believed to depict pronounced coastal

upwelling and high primary productivity conditions (Suess *et al.* 1988; Dunbar *et al.* 1990; Brand *et al.* 2004). Along the western bank of the Ica River, south and west of the Ocucaje village, two basin-wide erosional surfaces cut the Pisco strata, each reflecting a period of subaerial exposure and, as such, a break of the sedimentary history of the basin (Di Celma *et al.* 2017, 2018). Consequently, the Pisco Formation can be divided into three unconformity-bounded stratal packages (i.e., allomembers), designated P0, P1, and P2 in ascending stratigraphic order, which progressively onlap northeastwards a composite basal unconformity; each allomember consists of a coarse-grained lower portion, mostly comprised of nearshore gravels and sandstones, that passes upwards into an offshore interval of diatomaceous mudstones (Di Celma *et al.* 2017, 2018; DeVries & Jud 2018). The depositional age of the three Pisco allomembers in the study area has been recently constrained by means of diatom biostratigraphy, Ar-Ar radiochronology, and strontium isotope stratigraphy (Gariboldi *et al.* 2017; Bosio *et al.* 2019, 2020*a, b*): thus, P0 was deposited around 14.8-12.4 Ma (i.e., during the Langhian–Serravallian), P1 ca. 9.5-8.6 Ma (i.e., during the Tortonian), and P2 ca. 8.4-6.7 Ma (i.e., during the Tortonian–Messinian). These age estimates suggest that, at least in part, the deposition of the Pisco allomembers was, at least in part, controlled by glacio-eustatic fluctuations in sea-level (Di Celma *et al.* 2018).

All the specimens of the new inioid species described herein for which the stratigraphic whereabouts are known come from beds pertaining to the P1 allomember (referred to as the “Cerro Colorado lower allomember” by Di Celma *et al.* 2016). In particular, five stratigraphically framed finds are known from P1 exposures at the sites of Cerro Colorado (MUSM 565, MUSM 566, and MUSM 2541), south of Cerro la Bruja (MUSM 3902), and a locality informally named "Anfiteatro" by Bosio *et al.* (2020b) located between Cerro los Quesos and Cerros Cadena de los Zanjones (MUSM 3903); a sixth specimen, MUSM 2512, comes from undifferentiated Pisco strata cropping out at the locality

known as Corre Viento (a broad outcrop area, characterized by exposures of both the P1 and P2 allomembers, whose stratigraphic asset is nonetheless still largely unknown). The P1 stratal package exhibits its maximum thickness (ca. 100 m) in its southern exposures, in the vicinities of Cerros Cadena de los Zanjones and Cerros la Mama y la Hija, where they rest unconformably on P0 deposits (Di Celma *et al.* 2017, 2018). Towards the northeast, P1 thins significantly to become ca. 40 m thick at Cerro la Bruja, beyond which it is thought to disappear as a result of progressive northeastward onlap onto the basin basement (Di Celma *et al.* 2017). Some 30 km to the northwest of Cerro la Bruja, at Cerro Colorado, P1 is ca. 75 m thick, its lower boundary consisting of an angular unconformity with the underlying strata of the Chilcatay Formation (Di Celma *et al.* 2016).

The P1 allomember features a copious, diverse, and well-preserved fossil vertebrate assemblage that consists of cetaceans (including both mysticetes and odontocetes), pinnipeds, bony and cartilaginous fishes (including both sharks and rays), seabirds, crocodilians, and marine turtles (Parham & Pyenson 2010; Bianucci *et al.* 2010, 2016; Lambert *et al.* 2010*a, b*; Stucchi *et al.* 2016; Landini *et al.* 2017*a, b*; Ramassamy *et al.* 2018). Fossils of cetaceans are particularly numerous, the remains of baleen-bearing whales (consisting of a large-sized cetotheriid species and 2-3 balaenopterid species) being more abundant, but less diverse, than those of toothed whales (represented by two ziphiids, *Chimuziphius coloradensis* and *Messapicetus gregarius*, two physeteroids, *Livyatan melvillei* and *Acrophyseter* sp., two or more undescribed kentriodontid-like delphinidans, the pontoporiid inioid *Brachydelphis mazeasi*, the inioid *Brujadelphis ankylorostris*, and the new inioid taxon described herein). Cases of exceptional preservation from the deposits referred to the P1 allomember include the fossilized digestive tract contents of two cetaceans (a cetotheriid and a specimen of *Messapicetus gregarius*), revealing predation upon pilchards, and the phosphatised baleen of a balaenopterid whale (Collareta *et al.* 2015; Lambert *et al.* 2015; Gioncada *et al.* 2016).

MATERIAL AND METHODS

Institutional abbreviations

MUSM, Museo de Historia Natural, Universidad Nacional Mayor de San Marco, Lima, Peru.

Anatomical terminology

Terminology for skull anatomy follows Mead & Fordyce (2009), unless otherwise stated.

Phylogeny

To investigate its phylogenetic relationships the new taxon was coded in the character-taxon matrix of Lambert *et al.* (2018), modified from Geisler *et al.* (2011, 2012), Lambert *et al.* (2017), and Post *et al.* (2017), resulting in a matrix of 109 taxa and 324 characters (see Supplementary File 1 for the character-taxon matrix). As in previous analyses based on this matrix, we used Paup 4.0 (Swofford 2003); three outgroups (*Bos taurus*, *Hippopotamus amphibius*, and *Sus scrofa*) were defined; and ordered multistate characters were scaled for a minimum length of each being one step. Slightly differing from previous analyses, the constraint tree enforced as a backbone results from more recent maximum likelihood and Bayesian analyses of a very large genomic dataset on extant species (McGowen *et al.* 2019) (Supplementary File 2). Most parsimonious trees were obtained by heuristic search, using the tree-bisection-reconnection branch swapping algorithm and the ACCTRAN character-state optimization. Bootstrap values were calculated with Paup 4.0 (100 replicates).

SYSTEMATIC PALAEONTOLOGY

Order CETACEA Brisson, 1762

PELAGICETI Uhen, 2008

NEOCETI Fordyce & Muizon, 2001

Suborder ODONTOCETI Flower, 1867

Infraorder DELPHINIDA Muizon, 1984

Superfamily INIOIDEA Gray, 1846

Family PONTOPORIIDAE Kasuya, 1973

Remark on the family-level attribution. The new genus and species described herein is attributed to the family Pontoporiidae (defined as the clade grouping all the inioids more closely related to *Pontoporia* than to *Inia*), mostly based on the results of the phylogenetic analysis and one morphological feature, the anteroposterior elongation of the nasals typical for pontoporiids (Muizon 1984, 1988*a*). However, the support for this clade remains relatively low (see discussion below), and the topology of this part of the odontocete tree may change with the addition of taxa based on more complete specimens. More specifically, the discovery of new specimens for the new genus and species described herein (based on six cranial specimens), including the highly informative, but unfortunately easily detached ear bones

(especially the periotic), may confirm its attribution to the Pontoporiidae (see Muizon 1984, 1988*a*).

Samaydelphis gen. nov.

Derivation of name. From *samay*, intermediate in Quechua, referring to the cranial morphology of the new taxon being intermediate between the iniid *Inia* and the pontoporiid *Pontoporia*; and from *delphis*, dolphin in Latin.

Type species. *Samaydelphis chacaltanae* sp. nov.

Diagnosis. Same as for the only ~~referred~~ species until new species are described.

Samaydelphis chacaltanae sp. nov.

Figures 3-9

Derivation of name. The species name honours Ing. César Chacaltana-Budiel, geologist, director of Environmental Geology and former head of the Paleontology Area at the Instituto Geológico Minero y Metalúrgico (Ingemmet, Peru) for his constant support to the palaeontological study of marine vertebrate assemblages of the Pisco basin.

Holotype. MUSM 566, subcomplete cranium.

Type locality. Cerro Colorado, East Pisco basin, southern coast of Peru (see Bianucci *et al.* 2016; Di Celma *et al.* 2016) (Fig. 1). Geographic coordinates: 14°19'53.9" S, 75°54'06.8" W;

480 m above sea level. This specimen was reported in the Cerro Colorado fossil map of Bianucci *et al.* (2016) with the field number O25 and provisionally referred to as "Pontoporiidae n. sp."

Type horizon. Pisco Formation, P1 allomember ("Cerro Colorado lower allomember" in Di Celma *et al.* 2016), at 55.3 m above the contact with the underlying Chilcatay Formation (Fig. 2). This specimen is ca. 25 m above a radiometrically dated volcanic ash layer (CC-T1, 9.1 ± 0.04 Ma), ca. 20 m above the FO of *Koizumia tatsunokuchiensis* (9.0 Ma), ca. 3 m above the LO of *Lithodesmium reynoldsii* (8.9 Ma), and ca. 10 m below the LO of *Denticulopsis praekatayamae* (8.5 Ma). As such, diatom biostratigraphy and calculated $^{40}Ar/^{39}Ar$ ages converge to indicate an interval of deposition for the specimen-bearing strata between 8.9 and 8.5 Ma (Tortonian, early late Miocene).

Referred specimens. **MUSM 565**, subcomplete cranium, part of the axis and one thoracic vertebra. Cerro Colorado, Pisco Formation, P1 allomember, early late Miocene (9.5 - 8.6 Ma, Tortonian; see geological context above). Exact locality and stratigraphic horizon unknown. Approximate geographic coordinates: 14°20' S, 75°53' W. **MUSM 2541**, partial cranium including the rostrum base, the bony nares, the vertex, and part of the supraorbital regions, a fragment of mandible with several alveoli, and a few fragmented teeth. Cerro Colorado, Pisco Formation, P1 allomember, at 46.5 m above the contact with the underlying Chilcatay Formation (Fig. 2). This specimen is ca. 12 m above the FO of *Koizumia tatsunokuchiensis* (9.0 Ma) and ca. 5 m below the LO of *Lithodesmium reynoldsii* (8.9 Ma). As such, diatom biostratigraphy indicates an interval of deposition for the specimen-bearing strata spanning between 9.0 and 8.9 Ma (Tortonian). Geographic coordinates: 14°22'10.5" S, 75°52'41.3" W; 582 m above sea level. **MUSM 2512**, fragment of cranium including the vertex. Corre Viento

(Fig. 1), Pisco Formation, P1 or P2 allomember, late Miocene. Exact locality and stratigraphic horizon unknown. Approximate geographic coordinates: 14°27' S, 75°45' W. **MUSM 3902**, about 1 km south of Cerro la Bruja (Fig. 1) and 16 m below the holotype of *Brujadelphis ankylorostris*, Pisco Formation, P1 allomember, early late Miocene (9.5 - 8.6 Ma, Tortonian) (Fig. 2). Geographic coordinates: 14°33'16.8" S, 75°40'23.1" W. **MUSM 3903**, subcomplete cranium, Anfiteatro, Pisco Formation, P1 allomember, early late Miocene (9.5 - 8.6 Ma, Tortonian). The specimen has been collected ca. 25 m above a radiometrically dated volcanic ash layer (ANF-T1, 9.31 ± 0.01 Ma) (Fig. 2). Geographic coordinates: 14°32'55.41" S, 75°43'47.50" W, 582 m above sea level.

Diagnosis. This small size inioid (bizygomatic width between 144 and 153 mm) can be distinguished from other extinct and modern inioids by the following unique combination of morphological characters: proportionally short rostrum making 56-58 per cent of the condylobasal length; no lateral groove along the premaxilla-maxilla suture on the rostrum; narrow dorsal opening of the mesorostral groove along the whole rostrum length; shallow, anterolaterally open antorbital notch; no significant dorsoventral thickening of the lacrimal; premaxillary foramen posterior to the level of the antorbital notch; dorsoventrally high and transversely thick ridge along the anteromedial border of the posterolateral sulcus; moderately dorsoventrally thickened premaxillary eminence; extensive contact between the ascending process of the premaxilla and the corresponding nasal; vertex of the skull significantly higher than the premaxillary eminences; nasals roughly as transversely wide as the bony nares; nasals reaching the same dorsoventral height ~~than~~ the frontals on the vertex; no internasal fossa; long anteromedial projection of frontals between nasals on the vertex; long anteromedial projection of ?interparietal between frontals on the vertex; long anteromedial projection of the occipital shield between the maxillae; ventral margin of the occipital

condyles at about the same dorsoventral level as the ventral margin of the temporal fossa; broadly separated anterior apices of palatines; upper tooth count of about 30 teeth per row; at least 11 post-symphyseal teeth on the mandible; no lingual heel on the crown of posterior teeth; and transverse process of the axis being posterolaterally directed. See the discussion section for a more detailed comparison with extant and extinct inioids.

Description (Figs. 3-9)

General morphology of the cranium. With a bizygomatic width ranging from 144 to 153 mm (Table 1), *Samaydelphis chacaltanae* is a small-sized inioid, displaying a cranium that is significantly larger than in the extant *Pontoporia blainvillei*, slightly larger than in *Brachydelphis jahuayensis*, overlapping with the size interval of *Pliopontos littoralis* and *Brachydelphis mazeasi*, and smaller than in *Brujadelphis ankylorostris* and the extant *Inia geoffrensis* (Muizon 1984; Lambert & Muizon 2013; Lambert *et al.* 2017). Based on the stem delphinoid equation by Pyenson & Sponberg (2011) this range of bizygomatic widths corresponds to total body length estimates ranging between 1.48 and 1.56 m. The anterior tip of the rostrum is only preserved in MUSM 3902, where it is somewhat transversely flattened, but its anterior extent can be estimated in other rostra. The rostrum is pointed in dorsal view and proportionally short (Figs. 3, 5, 7; Table 1), accounting for about 56-58 per cent of the condylobasal length (mesorostrine condition sensu McCurry & Pyenson 2018), with a ratio between width at rostrum base and rostrum length ranging from about 0.38 to 0.42, thus being intermediary between the brevirostrine *B. mazeasi* and the longirostrine *B. jahuayensis*. Although showing a significant degree of variation in its dimensions, the rostrum of *Pontoporia* is considerably longer (Muizon 1984, table 1). At mid-length, the cross section of the rostrum is slightly wider than high. Differing from the other crania that comprise the studied sample, the rostrum of MUSM 565 curves slightly anterodorsally (Fig. 5), similar to

some specimens of *B. mazeasi* (Gutstein *et al.* 2009) and of a few other extinct and extant odontocetes (Bianucci *et al.* 2020). The temporal fossa is considerably anteroposteriorly longer (nearly two times) than the orbit, but its roof is much lower than the moderately elevated vertex (Figs. 3, 5, 7). The latter is transversely narrow (minimum distance between the maxillae across the vertex is lower than the width of the bony nares) (Figs. 3, 5-7), but not to the extent seen in *Meherrinia* (Geisler *et al.* 2012), *Pontistes* (Muizon 1984, fig. 18), and *Pontoporia*. The vertex reaches a significantly higher dorsoventral level than the dorsoventrally thick premaxillary eminences; this feature differs markedly from *Pliopontos* and *Pontoporia*, which display a much lower vertex. The facial region is moderately asymmetric, the vertex being distinctly shifted towards the left side in MUSM 565, 566, and, to a lesser degree, in MUSM 3903.

Premaxilla. Taking into account the incomplete apex of the rostrum in part of the studied specimens and the unfused lateral premaxilla-maxilla suture (anterior tip of the maxilla preserved in MUSM 565 and 566), we hypothesize that the premaxilla was originally at least 15-20 mm longer anteriorly than the maxilla. In specimen MUSM 3903, three anteriormost alveoli are tentatively identified in the premaxilla. The mesorostral groove is dorsally open in the anterior portion of the rostrum (Figs. 3, 5, 7). This dorsal window narrows somewhat towards the mid-part of the rostrum in MUSM 565, 566, and 3903, beyond which level it broadens to reach its maximum width just anterior to the level of the antorbital notches in MUSM 566, 2541, and 3903. The right and left premaxillae contact (or almost contact) each other on the anterior margin of the anteroposteriorly short bony nares, providing this margin with a U-shape. No conspicuous dorsal exposure of the presphenoid is observed in this area. Along the rostrum, each premaxilla gradually widens towards the rostrum base, where the premaxilla is markedly wider than the maxilla in dorsal view. There is no lateral groove along

the rostral premaxilla-maxilla suture, a marked difference with *Pliopontos* and *Pontoporia*.

From the level of the antorbital notch, the lateral margins of the premaxillae more abruptly diverge posterolaterally, thus resulting in a distinctly laterally convex outline in the facial region. The dorsal surface of the premaxilla rises posterodorsally from the level of the antorbital notch, anterior to the premaxillary eminence. The premaxillary foramen is located posterior to the antorbital notch, in a depressed triangular region that is especially excavated in MUSM 566 and 2541. The anteromedial sulcus is long and deep in its proximal portion, especially in MUSM 2541 and 3903, where it is shaped as a deep longitudinal slit. The posterolateral sulcus turns posterolaterally and then posteriorly, following the curve of the lateral margin of the premaxilla. Its proximal part is also deep, related to the development of a dorsoventrally high and transversely thick ridge along its anteromedial border. This ridge is conspicuous in MUSM 565, 566, 2541, and 3902, and probably present but partly worn in MUSM 3903. The posterolateral sulcus becomes shallower posterolaterally, along the premaxillary eminence, but it reaches at least the mid-length of the bony nares. The prenarial triangle is transversely concave to flat, with its medial edge rising dorsomedially in MUSM 566, 2541, and 3902. The posteromedial sulcus is barely defined, rising posteromedially towards the anteromedial margin of the bony nares. The premaxillary eminence is anteroposteriorly short (corresponding to a short distance between the premaxillary foramen and bony naris, as for example in *Brachydelphis mazeasi*) and moderately dorsoventrally thickened, although to a lesser degree than in *Scaldiporia* (Post *et al.* 2017). Its maximum height is observed along the anterior half of the bony naris. The lateral flank of the eminence is higher in MUSM 565, 566, and 3903, being nearly vertical on the right side of MUSM 565 (Figs. 4, 5). Turning around the corresponding bony naris, each eminence gradually lowers and narrows posteriorly. As in other inioids, no significant asymmetry could be noted between left and right premaxillary eminences, whereas the overlying posterior part of the melon is

highly asymmetric in *Pontoporia*, with a greatly reduced left branch (Frainer *et al.* 2015). From the mid-length of the bony nares, the premaxillae rise again and converge posterodorsomedially to contact the anterolateral corners of the nasals, thus being reminiscent of the condition observed in *Awadelphis*, *Brachydelphis*, and *Pontistes*. The medial margin of the ascending process of the premaxilla does not diverge laterally along the bony naris, thus not leading to a medial exposure of the maxilla along the naris. In all the analyzed specimens, the tongue-shaped posterior end of the premaxilla contacts the nasal along the anterolateral flank of the vertex on both sides of the skull, for a width of 7-10 mm (Figs. 3, 5-7), a plesiomorphic condition differing markedly from *Auroracetus*, *Brujadelphis*, *Inia*, *Meherrinia*, *Pliopontos*, *Pontoporia*, *Scaldiporia*, and *Stenasodelphis*, which all lack such a contact (see Frainer *et al.* 2015, fig. 7 for a visualization of this character at different ontogenetic stages in *Pontoporia*).

Maxilla. In dorsal view, the maxilla is exposed lateral to the premaxilla for most of the rostrum length (Figs. 3, 5, 7). Its medial margin is subvertical at the anterior end of the rostrum; posteriorly, it gradually shifts to a more dorsolateral orientation, before reducing its dorsoventral height from a level 30-40 mm anterior to the antorbital notch, as best seen in lateral view. The posteriormost portion of the lateral edge of the rostrum remains dorsoventrally thick in close vicinity of the notch. In dorsal view, a slight lateral expansion of the rostrum is observed in MUSM 565, 566, and 3903, a few centimeters anterior to the notch; it is weaker than in *Parapontoporia* spp. and the recently extinct *Lipotes vexillifer* and (see Barnes 1985).

The antorbital processes of the maxillae are better preserved in MUSM 566, in which the left antorbital notch is deeper, related to a longer antorbital process (Fig. 3). Even there, the notch remains shallow (4.5 mm) and broadly anterolaterally open, differing from the

deeper notch in *Brachydelphis*, *Inia*, *Isthminia*, *Pliopontos*, *Pontoporia*, and *Stenasodelphis*. The right notch of MUSM 566 is nearly completely open laterally, as observed in part of the phocoenids. The antorbital notches are, similarly, roughly directed transversely in other specimens, except for the right antorbital notch of MUSM 565 being slightly deeper and followed posteriorly by a short groove. A small dorsal infraorbital foramen is visible at the level of the antorbital notch on both sides of MUSM 566, on the right side of MUSM 3902, and on the left side of MUSM 3903 (Figs. 3, 7). A few additional small foramina are probably present, in a more anterior position, along the maxilla-premaxilla suture. Posterolateral to the antorbital notch, the dorsal surface of the maxilla is thickened, marking the start of a low and generally transversely thin maxillary crest, directed posteriorly and slightly laterally towards the postorbital process, and being less developed than in *Pontoporia*. The crest is less well defined in MUSM 566. The area of the maxilla between the crest and the premaxilla is slightly depressed. From the level of the postorbital process backwards, the surface of the maxilla is transversely concave, with a slightly elevated lateral margin (less so than in *Inia*) (Figs. 4, 5). A tiny posterior dorsal infraorbital foramen (diameter 3-4 mm) is found in all specimens at a short distance (5-7 mm) from the premaxilla-maxilla suture and at the anteroposterior level of the postorbital process (or slightly anterior). The slightly raised lateral margin of the maxilla turns posteromedially above the temporal fossa before joining the nuchal crest. The latter is higher and turns smoothly, anteromedially, towards the vertex. The maxilla reaches a level significantly posterior to the anteromedial margin of the supraoccipital, the nuchal crest drawing a deep double wave in dorsal view. The whole posterior part of the maxilla is transversely concave, more so in MUSM 565 than in other specimens. The medial margin of the maxilla rises against the vertex, with the right side being more erect (i.e., roughly vertical) in part of the specimens (MUSM 566, 2541, 3902, and 3903).

The maxillary alveoli are generally poorly preserved. In MUSM 565, the anterior alveoli display a transverse diameter of 5 mm and an interalveolar septum of 1.5-2 mm (Fig. 5). In MUSM 3902, 21 alveoli are counted on a length of 95 mm on the posterior part of the left alveolar groove, with diameters of 3-5 mm and septa shorter than 1 mm. Combining partial alveolar counts in MUSM 3902 (posteriorly) and MUSM 3903 (anteriorly), we estimate the upper tooth count at about 30, in the range of *Inia* and *Lipotes*, but lower than in *Pontoporia* (Best & da Silva 1989; Brownell 1989; Chen 1989). The alveolar groove ends 20-22 mm anterior to the antorbital notch in MUSM 3902 and 3903. The ventral surface of the rostrum is marked by a median ~~through~~, where the keeled ventral exposure of the vomer appears for about 30 mm in MUSM 3902. Anterior to the pterygoid sinus fossae, the surface of the palate is broad and flat. Lateral to the palatine, a shallow fossa with a rounded anterior outline excavates the rostrum base until a level 20-25 mm anterior to the antorbital notch (Figs. 4, 5). Also observed in *Inia* and *Pontoporia*, this fossa probably corresponds to the area of origin for the m. pterygoideus internus (see Seagars 1982). The interpretation of this fossa as housing the anterior sinus appears less likely, considering the markedly different outline of this sinus, as reported by Fraser & Purves (1960) in *Inia*, *Lipotes*, and *Pontoporia*. Best seen in MUSM 566 and 3903, the ventral infraorbital foramen is anteroposteriorly long (21 mm on the right side of MUSM 566).

Nasal. The nasals are prominent anterodorsally on the vertex, reaching a much higher dorsoventral level than the cribriform plate, the latter being lower than the posterodorsal tip of the premaxilla. In lateral view, the anterior wall of the nasal draws an angle of approximately 45° with the horizontal, sloping anteroventrolaterally, a condition reminiscent of *Meherrinia*. Each nasal is either slightly higher than the corresponding frontal (in MUSM 2541 and 3902) or roughly at the same level (in MUSM 565, 566, and 3903), thus differing from *Inia*,

Ischyrorhynchus, and *Kwanzacetus*, which display significantly lower nasals. In dorsal view, the nasals are as wide as the bony nares (a difference with *Meherrinia*, which bears narrower nasals) and wider than the frontals (to an even greater extent in MUSM 3902, whose posterior part of the vertex is more transversely pinched) (Figs. 3, 5-7). The difference of width between nasals and frontals on the vertex is not as great as in *Brachydelphis mazeasi*, *Brujadelphis*, *Isthminia*, *Pontistes*, *Pontoporia*, and *Scaldiporia*, in which the posterior part of the vertex is even more pinched. The anterior margin of each nasal is transversely concave, with the anteromedial corner being significantly longer anteriorly than the anterolateral corner. The dorsal surface of the nasals and frontals on the vertex is roughly flat in MUSM 565, 566, 2541, 2512, and 3903, whereas the nasals bulge dorsally in MUSM 3902. In MUSM 2541, and to a lesser extent MUSM 2512, each nasal bears a well-defined facet, located anterolaterally, being slightly concave, and facing dorsolaterally. No conspicuous internasal fossa is observed in any specimen, a marked difference with *Pontistes* and *Pontoporia*.

Frontal. On the vertex, each frontal sends a long and narrow projection between the nasals in MUSM 565, 566, and 3903; the projection is even longer in MUSM 2541 and MUSM 2512, making one third to one half of the length of the nasal (feature not visible in MUSM 3902) (Figs. 3, 5-7). A narrow anteromedial projection of the frontals is also observed in *Brachydelphis*, *Meherrinia*, *Pliopontos*, *Pontistes*, *Pontoporia*, and *Stenasodelphis*, but it is generally shorter (except for some specimens of *Meherrinia*). The dorsal surface of the frontals is slightly depressed medially in MUSM 565, 566, and 2541. There is no frontal boss (or frontal hump, see Muizon 1988*b*), a major difference with *Inia*, *Ischyrorhynchus*, and *Kwanzacetus*.

The preorbital process of the frontal is moderately dorsoventrally thickened, more so in MUSM 565 and 566 than in MUSM 3902 (Figs. 3, 5, 7). The orbit is short compared to the temporal fossa, but less reduced than in *Inia*. The pointed postorbital process extends ventrally and slightly posterolaterally; it displays a robust base, with a triangular cross section due to the development of the lateral part of the infratemporal crest. The latter is more poorly individualized at mid-width of the frontal in ventral view; more medially, it makes a thin and high crest for the posterior wall of the frontal groove, which is best seen in MUSM 566. At least in MUSM 566 and 3903, posterior to the frontal groove, the medial part of the ventral surface of the frontal is deeply excavated, displaying a large fossa for the postorbital lobe of the pterygoid sinus that is not clearly defined laterally but that deepens somewhat dorsomedially.

The temporal fossa is only partly roofed by the frontal and maxilla; consequently, its laterally inflated medial wall is visible in dorsal view for the posterior third of its length.

Lacrimojugal complex. In most specimens, the base of the styliform process of the jugal is preserved, just posterior to the antorbital notch. In ventral view of the left side of MUSM 3903, the medial suture of the jugal with the maxilla is visible, running posteriorly at some distance from the anterolateral margin of the infraorbital foramen. The lacrimal-frontal suture is best seen in ventral view on the left side of MUSM 566, projecting from the anterolateral margin of the preorbital process in a posteromedial direction, before turning medially (Fig. 4). The lacrimojugal complex is barely dorsoventrally thickened in the antorbital region (Figs. 3, 5, 7), differing markedly from the dorsoventrally high complex seen in *Brachydelphis* (see Muizon 1988*a*; Lambert & Muizon 2013).

Palatine and pterygoid. The palatine-maxilla suture is difficult to follow: partly visible on the right side of MUSM 566, it runs anteromedially until a level 33 mm anterior to the corresponding antorbital notch, beyond which level it abruptly turns posteromedially. The apices of the right and left palatines are thus broadly (about 20 mm) separated from each other, a condition similar to that observed in MUSM 565 (Figs. 4, 5) and differing from the closely appressed apices of *Pliopontos* and, to a lesser extent, *Inia*. Anteromedial to the tip of the palatine, a major palatine foramen is seen on both sides of MUSM 565, 566, and 3903. The pterygoid sinus fossa reaches an anteroposterior level just anterior to the level of the antorbital notches. The anterior part of the fossa is shallow, and the fossa deepens markedly towards the anterior margin of the adjoining choana. The lateral lamina of the palatine ends at about mid-length of the choana.

There is no indication for a long lateral lamina of the pterygoid in any specimen, whereas the medial lamina is preserved in several of them. *Samaydelphis* most likely differs from the living *Pontoporia* in the absence of such an extended lateral lamina of the pterygoid.

Interparietal. On the vertex, a small, roughly triangular bone unit is exposed, along the sagittal plane, between the supraoccipital and the frontals. From the nuchal crest it projects anteromedially, displaying either a V-shaped (MUSM 565, 566, 3902, and 3903) or W-shaped suture (MUSM 2512 and 2541) with the frontals (Figs. 3, 5-7). Not being crossed by a sagittal suture in MUSM 2541, 2512, and 3903 (region not optimally preserved in MUSM 565, 566, and 3902), this bony unit does not seem to correspond to a paired bone; therefore, as in *Stenasodelphis* (see Godfrey & Barnes 2008), we interpret it as a dorsal exposure of the interparietal, which among odontocetes generally fuses with the supraoccipital early in ontogeny (Mead & Fordyce 2009). A more dorsally protruding sagittal bony element,

observed in *Kwanzacetus* and several specimens of *Inia*, was similarly interpreted as part of the interparietal (Lambert *et al.* 2018).

Supraoccipital. As mentioned above, the occipital shield projects far anteromedially between the maxillae, as in *Meherrinia* and *Pliopontos*; characterized by a rounded anterior outline in dorsal view, the anteroposterior extent of this projection ranges from 16 mm (in MUSM 565) to 23 mm (in MUSM 566) (Figs. 3, 5-7). As a consequence of this projection and of the highly posterodorsally inflated brain hemispheres, the dorsomedial surface of the supraoccipital is subhorizontal and separated from the nuchal crest by a clear step. The upper part of the occipital shield is transversely and dorsoventrally convex. A sagittal groove marks the lower two thirds of its height in MUSM 565, 566, 2541, and 3903; the groove is deeper in MUSM 565, and broader and shallower in MUSM 566 and 3903. Due to the posteromedial extension of each temporal fossa, the occipital shield is moderately pinched transversely at mid-height, with the posteromedialmost part of the low temporal crest being close to the corresponding occipital condyle (Figs. 4, 5). Narrow but deep dorsal condyloid fossae are observed.

Squamosal. The zygomatic process of the squamosal is interpreted as roughly complete on the left side of MUSM 565, on the right side of MUSM 3902, and possibly on the left side of MUSM 566 (Figs. 3, 5, 7). It is long and slender, being directed anterodorsally towards the postorbital process of the frontal. Especially conspicuous in MUSM 3902 (Fig. 7), the dorsoventral tapering of the zygomatic process towards its apex is strongly reminiscent of the condition of *Pontoporia*, differing markedly from the apical dorsoventral thickening observed in *Brujadelphis*, *Inia*, and *Isthminia*. The zygomatic process of *Pliopontos* and, to a greater extent, *Brachydelphis* appears as a whole more dorsoventrally thickened. On the left side of

MUSM 565, the distance between the anterior tip of the zygomatic process and the ventral tip of the postglenoid process is 50 mm. In lateral view, its dorsal edge is slightly convex whereas its ventral edge is slightly concave. Its lateral surface is excavated by a broad longitudinal groove. The postglenoid process is short, ending ventrally as a moderately thick, transversely directed crest. The posttympanic process is anteroposteriorly short (about 14 mm long on the left side of MUSM 565). The floor of the squamosal fossa is slightly sigmoid along its anteroposterior axis, being convex anteriorly and concave posteriorly.

~~In ventral view,~~ the mandibular fossa is broad and anteroventrally facing. The tympanosquamosal recess extends dorsomedial to the mandibular fossa, on the medial surface of the postglenoid process, and anterolaterally along the medial part of the ventral surface of the zygomatic process, with a lateral boundary fading away before mid-length of the process (Figs. 4, 5). The falciform process (best seen in MUSM 565 and 566) is shaped as a large blade extending over 22-23 mm from the mandibular fossa in an anteromedial direction. The foramen ovale is visible on both sides of MUSM 3903, opening laterally and slightly posteriorly, but the squamosal-alisphenoid suture could not be distinguished.

Exoccipital. The posterior surface of the exoccipital is overhung by the posteromedially protruding temporal crest. This surface is directed laterally and dorsoventrally concave. The occipital condyles are located at a dorsoventrally low position on the posterior wall of the neurocranium; their ventral margin is at about the ventral level of the temporal fossa (Figs. 3-5, 7). However, this is not as low as in *Brachydelphis*, *Inia*, *Kwanzacetus*, *Pontoporia*, and *Scaldiporia*. The articular surfaces of the condyles face posteroventrally.

Basioccipital. Better preserved in MUSM 565 (Fig. 5), the basioccipital crests are slender and moderately diverge posterolaterally (drawing an angle of about 35° with each other), only gradually thickening distally.

Mandible. The 61-mm-long fragment of the right mandible of MUSM 2541 corresponds to a section just posterior to the mandibular symphysis (Fig. 8). It includes 11 complete to partly preserved alveoli, with a transverse diameter ranging from 6 to 7 mm and interalveolar septa 1-1.5 mm thick. The minimum post-symphyseal tooth count is, as in *Pliopontos*, higher than in *Inia*, *Isthminia*, and *Pontoporia*. No longitudinal groove is observed along the lateral surface of this fragment, but the ventralmost part is missing and a curved region of the preserved ventral edge could correspond to the posterior end of such a groove, as seen in *Pontoporia*; alternatively, a large mental foramen may have been originally present in this region. Posterodorsal to this curved margin, a small mental foramen is observed, as, for instance, in *Brujadelphis*, *Inia*, and *Isthminia*.

Teeth. Only a few, partly complete single-rooted teeth of MUSM 2541 are preserved. One of them, most likely a posterior lower tooth, is at least 13.8 mm long and displays a conical, short crown (ratio between basal diameter and height = 0.7) whose apex curves distinctly lingually (Fig. 8). Based on its crown proportions and curvature this tooth is interpreted as originating from the posterior part of the tooth row. It lacks the typical strong lingual heel observed on the crown of posterior teeth in *Inia*. The enamel surface is slightly ornamented with numerous low ridges, which are less prominent than in *Inia* and the extinct iniid *Kwanzacetus* (Lambert *et al.* 2018).

Vertebrae. The epiphyses of the centrum are fused in both the axis (posterior epiphysis) and a thoracic vertebra (anterior and posterior epiphyses) of MUSM 565 (Fig. 9), suggesting that the represented individual was at least a few years old (see Galatius & Kinze 2003; Moran *et al.* 2014); however, additional vertebrae would be needed to provide more precise clues on the ontogenetic stage of this individual.

The neural arch of the axis is missing, but the rest of the bone is finely preserved. Anterior articular facets with the atlas indicate that the two first cervical vertebrae were not fused, a condition found in all other extant and extinct inioids for which this region is preserved (Van Beneden & Gervais 1880; Miller 1918; Muizon 1984; Lambert *et al.* 2017, 2018). The odontoid process is robust. The posterior epiphysis is distinctly pointed ventrally. The transverse process is robust and extends far beyond the lateral margin of the anterior articular facet for the atlas in a posterolateral direction; it is laterally longer than in *Inia* (Table 2) and differs from *Pontoporia* and *Lipotes* in not being ventrolaterally directed, being more similar to *Pliopontos*.

The preserved thoracic vertebra has a centrum that is longer than wide or high (Table 2). It displays a transverse process that is at approximately the same dorsoventral height compared to the centrum as in the thoracic T10 of *Pliopontos* (Muizon 1984), but the process is proportionally markedly shorter in MUSM 565, possibly indicating a more anterior position along the thoracic segment of the vertebral column. It is worth noting that vertebrae from the mid-thoracic region bear even shorter transverse processes in *Inia* and *Pontoporia* (Flower 1867; Van Beneden & Gervais 1880).

PHYLOGENY

As in previous cladistic analyses based on an earlier version of our character-taxon matrix, inioid species based on relatively fragmentary material and/or more specifically missing the ear bones tend to be highly versatile in obtained trees (Post *et al.* 2017; Lambert *et al.* 2018). For that reason, following preliminary tests we removed nine of these taxa (*Auroracetus bakerae*, *Ischyrorhnychus vanbenedeni*, *Isthminia panamensis*, *Kwanzacetus khoisani*, *Lophocetus calvertensis*, *Pithanodelphis cornutus*, *Protophocaena minima*, *Scaldiporia vandokkumi*, and *Stenasodelphis russellae*) from our analysis, totaling 97 ingroup taxa. The phylogenetic relationships of the taxa listed above were individually tested and commented in previous analyses (see, e.g., Geisler *et al.* 2012; Pyenson *et al.* 2015; Post *et al.* 2017; Lambert *et al.* 2017, 2018; Peredo *et al.* 2018), and we anticipate that only the discovery of new specimens with ear bones associated will allow for the relationships of all these taxa to be convincingly assessed in a single analysis. The heuristic search with a molecular constraint on extant species applied as a backbone resulted in a single most parsimonious tree with tree length = 2021.48, CI = 0.16, and RI = 0.56 (Fig. 10; Supplementary File 3 for the complete tree). In this tree *Samaydelphis chacaltanae* is recovered as sister-group to *Meherrinia*, being more distantly related to a monophyletic *Brachydelphis mazeasi* + *Brachydelphis jahuayensis*, *Pliopontos*, and the extant *Pontoporia* in the family Pontoporiidae. *Brachydelphis*, *Pliopontos*, and *Pontoporia* were similarly forming a clade in the analyses by Lambert *et al.* (2017), Post *et al.* (2017), and Lambert *et al.* (2018). As in two previous analyses *Brujadelphis* falls within Iniidae (Lambert *et al.* 2018; Post *et al.* 2017). The general topology for Inioidea is similar to the one recovered by Lambert *et al.* (2018), differing from Post *et al.* (2017) in excluding *Atocetus* spp. from that superfamily; members of this genus fall among stem delphinidans, together with a series of taxa previously referred to the family Kentriodontidae. As in Peredo *et al.* (2018), but with a lower number of sampled taxa, Kentriodontidae is reduced to a less inclusive clade of stem delphinidans, including here

Kentriodon and *Rudicetus*. Differing from Peredo *et al.* (2018), *Kampholophos* appears here as more closely related to *Hadrodelphis* and *Macrokentriodon* than to *Kentriodon* and *Rudicetus*. It is worth noting that (1) support is generally low for the recovered delphinidan clades (bootstrap values < 50, except for lipotids) and (2) the deletion of more fragmentarily known taxa considerably limits the size of the analysed sample. More complete specimens will be needed to further improve our understanding of inioid (and, more broadly, early delphinidan) phylogenetic relationships.

DISCUSSION

Among inioids, *Samaydelphis chacaltanae* differs from *Inia* and the closely related iniids *Ischyrorhynchus* and *Kwanzacetus* in the absence of a frontal boss and the nasals reaching the same dorsal height as the frontals on the vertex, from *Inia* and *Ischyrorhynchus* in the lack of a marked ornamentation of dental enamel, and from *Inia* in the absence of a lingual heel on posterior teeth. Along with *Brujadelphis* and *Isthminia* (both recovered as iniids in previous phylogenies, as well as in the present work; Pyenson *et al.* 2015; Lambert *et al.* 2017, 2018) it further differs from the taxa listed above in the retention of a premaxilla-nasal contact. *Samaydelphis* shares with *Pontoporia*, as well as with several other inioids generally identified as pontoporiids (*Auroracetus*, *Brachydelphis*, *Pliopontos*, *Pontistes*, *Protophocaena*, *Scaldiporia*, and *Stenasodelphis*; Muizon 1984, 1988*a*; Lambert & Post 2005; Godfrey & Barnes 2008; Gibson & Geisler 2009; Lambert & Muizon 2013; Post *et al.* 2017), nasals that are anteroposteriorly elongated and reach the same dorsal height as the frontals on the vertex. Here again, it differs from most of the listed taxa (except *Brachydelphis*, *Pontistes*, and the more fragmentarily known *Awadelphis*) in the retention of a

premaxilla-nasal contact, most likely representing the plesiomorphic condition for early delphinidans. It further differs from *Pliopontos* and *Pontoporia* in the vertex reaching a considerably higher dorsoventral level than the premaxillary eminences.

The highly unusual and distinctive lowering of the vertex observed in *Pliopontos* and *Pontoporia* has recently been investigated in relation with the soft anatomy of the forehead in the latter. In this genus, the low vertex is related to a relatively dorsoventrally low position of the bursae, soft tissue structures involved in the production of high frequency sounds (Huggenberger *et al.* 2010). Coupled with a relatively lower encephalization quotient in *Pontoporia* (compared to *Tursiops*, for example), the low position of the bursae has been tentatively correlated to the elongation of the whole nasal complex; in turn, such an elongation of the acoustic pathway may have helped focusing sounds (Huggenberger *et al.* 2010). The fact that earlier inioids display a higher vertex compared to *Pontoporia* supports the idea that the condition observed in the latter is a derived feature, only present in a few, later pontoporiids. Its presence in *Pliopontos littoralis* allows us to trace the origin of this major change in pontoporiid cranial topography as far back as the late Miocene (Sud-Sacaco vertebrate level, Sacaco Basin, Messinian; Muizon, 1984; Ehret *et al.* 2012; Lambert & Muizon 2013). Interestingly, neonates of *Pontoporia* display premaxillary eminences that are distinctly lower than the vertex (see Frainer *et al.* 2015, fig. 3), as in adults of many extinct inioids (including *Samaydelphis chacaltanae*), thus differing markedly from the adult condition and suggesting that the ancestral cranial topography is retained in early ontogenetic stages of *Pontoporia*.

The combination of anteroposterioly elongated nasals, reaching the same dorsal height as the frontals on the vertex, with a transversely pinched vertex, an extended anteromedial projection of the frontals between the nasals (reduced in part of the specimens), and an extended anteromedial projection of the supraoccipital between the maxillae has also been

observed in the geologically younger *Meherrinia*, represented by nine fragmentary crania, all of which only displaying the vertex, bony nares, and part of the supraorbital processes (Geisler *et al.* 2012), from the Messinian of North Carolina. However, it differs significantly from *Samaydelphis* in lacking a premaxilla-nasal contact. Tentatively referred to the family Iniidae in its initial study (Geisler *et al.* 2012) *Meherrinia* was recovered as more closely related to *Inia geoffrensis* by Pyenson *et al.* (2015) and as a stem inioid by Murakami (2016). Considering that our phylogenetic analysis supports a sister-group relationship with *Samaydelphis* (Fig. 10), *Meherrinia* is here tentatively included in the family Pontoporiidae. The generally more complete inioid material from the late Miocene of the Pisco Basin here again confirms its pivotal position for the elucidation of phylogenetic relationships for more fragmentarily known inioid taxa discovered outside Peru.

Furthermore, the description of this new genus and species from the Pisco Formation further increases the diversity of inioids in the southeastern Pacific during the late Miocene. Indeed, *Samaydelphis chacaltanae* represents the fourth inioid species recorded from late Miocene levels of the Pisco Formation. Furthermore, at least three of these four species (*Brachydelphis mazeasi*, *Brujadelphis ankylorostris*, and *S. chacaltanae*) originate from the stratal package P1. These three species were coeval in a restrict interval of time spanning from 9.31 ± 0.01 Ma ($^{40}Ar/^{39}Ar$ age of the volcanic ash layer ANF-T1) and 8.5 Ma (LO of *Denticulopsis praekatayamae*) or 8.6 ± 0.11 Ma ($^{40}Ar/^{39}Ar$ age of the volcanic ash layer ZANJ-T3 from Cerros Cadenas de los Zanjones) (Fig. 2). *B. mazeasi* is also found in the uppermost portion of P1 and in stratigraphically higher layers of the P2 allomember (Di Celma *et al.* 2017; Gioncada *et al.* 2018; pers. obs.). In particular, the stratigraphically younger specimen of *B. mazeasi* that we found in the P2 allomember is a skull from Cerro Hueco la Zorra, about 12 km north of Cerro la Bruja. The age of this specimen can be constrained by combining the lithostratigraphic markers mapped by Di Celma *et al.* (2018)

and radiometric ages obtained by two volcanic ash layers (Bosio *et al.* 2019, 2020b). The skull has been collected in the sediment package bounded by the P2-6 marker below and the P2-7 marker above. At Cerro la Bruja, a volcanic ash layer (LB-T11) located about 5 m above P2-6 yielded a radiometric age of 7.45 ± 0.01 Ma, whereas at Cerro Hueco la Zorra a second ash layer (LZ-T1) placed about 25 m above P2-7 gave a radiometric age of 7.155 ± 0.015 Ma. Therefore, the age of this specimen spans between 7.45 and 7.155 Ma. From a geographic point of view, *S. chacaltanae* was found together with *B. mazeasi* at Cerro Colorado (Bianucci *et al.* 2016*b*; this work), Corre Viento (Gioncada *et al.* 2018; this work), Cerros Cadena de los Zanjones (AC, GB, OL, pers. obs. 2013-16; this work), and, also with *B. ankylorostris* south of Cerro la Bruja (Lambert *et al.* 2017; AC, GB, OL, pers. obs. 2013-16; this work).

In addition to size differences (with a bizygomatic width of about 210 mm *B. ankylorostris* is significantly larger than both *B. mazeasi* and *S. chacaltanae*), these three species differ in the proportions of their rostrum (Fig. 11), ranging from the brevirostrine *B. mazeasi* to the mesorostrine *S. chacaltanae*, and the longirostrine *B. ankylorostris* (categories *sensu* McCurry & Pyenson 2018). In relation to its markedly shorter rostrum *B. mazeasi* differs in its lower tooth count (ca 22 vs. ca 30 in the two other taxa), whereas the larger *B. ankylorostris* displays more robust teeth on a stronger rostrum. All these differences suggest that these three sympatric species of inioids used different feeding strategies (for example, with a greater contribution of suction in the brevirostrine *B. mazeasi*; see Werth 2006; Lambert & Muizon 2013) and/or could target different prey sizes.

Acknowledgements. We wish to warmly thank W. Aguirre for the careful preparation of specimens of the new genus and species *Samaydelphis chacaltanae* at MUSM, R. Salas-

Gismondi and R. Varas-Malca for greatly facilitating our work at MUSM, S. Bruaux and O. Pauwels (IRSNB, Brussels, Belgium), S. J. Godfrey and J. R. Nance (CMM, Solomons, USA), C. Lefèvre (MNHN, Paris, France), S. Farina (MSNUP, Pisa, Italy), R. Salas-Gismondi and R. Varas-Malca (MUSM, Lima, Peru), H. van der Es (NMR, Rotterdam, The Netherlands), D. J. Bohaska, J. G. Mead, C. W. Potter, and N. D. Pyenson (USNM, Washington DC, USA), and Z. Gasparini and L. H. Pomi (MLP, La Plata, Argentina) for access to collections under their care. This project received funding from the University of Pisa (PRA_2017_0032) to G.B., from the Italian Ministero dell'Istruzione, dell'Università e della Ricerca (MIUR) (PRIN Project, 2012YJSBMK EAR- 9317031) to G.B., and from the National Geographic Society Committee for Research Exploration (GEFNE 177-16) to O.L.

REFERENCES

AGUIRRE-FERNÁNDEZ, G., MENNECART, B., SÁNCHEZ-VILLAGRA, M. R., SÁNCHEZ, R. and COSTEUR, L. 2017. A dolphin fossil ear bone from the northern Neotropics–insights into habitat transitions in iniid evolution. *Journal of Vertebrate Paleontology*, **37**, e1315817.

BARNES, L. G. 1985. Fossil pontoporiid dolphins (Mammalia, Cetacea) from the Pacific Coast of North America. *Los Angeles County Museum Contributions in Science*, **363**, 1-34.

BEST, R. C. and DA SILVA, V. M. F. 1989. Amazon river dolphin, Boto. *Inia geoffrensis* (de Blainville, 1817). 1-23. *In* RIDGWAY, S. H. and HARRISON, R. (eds). *Handbook of marine mammals, vol. 4: River dolphins and the larger toothed whales*. Academic Press, London.

BIANUCCI, G., LAMBERT, O. and POST, K. 2010. High concentration of long-snouted beaked whales (genus *Messapicetus*) from the Miocene of Peru. *Palaeontology*, **53**, 1077-1098.

BIANUCCI, G., DI CELMA, C., COLLARETA, A., LANDINI, W., POST, K., TINELLI, C., DE MUIZON, C., BOSIO, G., GARIBOLDI, K., GIONCADA, A., MALINVERNO, E., CANTALAMESSA, G., ALTAMIRANO-SIERRA, A., SALAS-GISMONDI, R., URBINA, M. and LAMBERT, O. 2016*a*. Fossil marine vertebrates of Cerro Los Quesos: Distribution of cetaceans, seals, crocodiles, seabirds, sharks, and bony fish in a late Miocene locality of the Pisco Basin, Peru. *Journal of Maps*, **12**, 1037-1046.

BIANUCCI, G., DI CELMA, C., LANDINI, W., POST, K., TINELLI, C., DE MUIZON, C., GARIBOLDI, K., MALINVERNO, E., CANTALAMESSA, G., GIONCADA, A., COLLARETA, A., SALAS-GISMONDI, R., VARAS-MALCA, R., URBINA, M. and LAMBERT, O. 2016*b*. Distribution of fossil marine vertebrates in Cerro Colorado, the type locality of the giant raptorial sperm whale *Livyatan melvillei* (Miocene, Pisco Formation, Peru). *Journal of Maps*, **12**, 543-557.

BIANUCCI, G., MUIZON, C. DE, URBINA, M., and LAMBERT, O. 2020. Extensive diversity and disparity of the early Miocene platanistoids (Cetacea, Odontoceti) in the southeastern Pacific (Chilcatay Formation, Peru). *Life*, **10**, 27.

BOSIO, G., GIONCADA, A., MALINVERNO, E., DI CELMA, C., VILLA, I. M., CATALDI, G., GARIBOLDI, K., COLLARETA, A., URBINA, M. and BIANUCCI, G. 2019. Chemical and petrographic fingerprinting of volcanic ashes as a tool for high-resolution stratigraphy of the upper Miocene Pisco Formation (Peru). *Journal of the Geological Society*, **176**, 13-28.

BOSIO, G., MALINVERNO, E., COLLARETA, A., DI CELMA, C., GIONCADA, A., PARENTE, M., BERRA, F., MARX, F. G., VERTINO, A. and URBINA, M. 2020*a*.

Strontium Isotope Stratigraphy and the thermophilic fossil fauna from the middle Miocene of the East Pisco Basin (Peru). *Journal of South American Earth Sciences*, **97**, 102399.

BOSIO, G., MALINVERNO, E., VILLA, I. M., DI CELMA, C., GARIBOLDI, K., GIONCADA, A., BARBERINI, V., URBINA, M. and BIANUCCI, G. 2020*b*. Tephrochronology and chronostratigraphy of the Miocene Chilcatay and Pisco formations (East Pisco Basin, Peru). *Newsletters on Stratigraphy*, **53**, 213-247.

BRAND, L., ESPERANTE, R., CHADWICK, A. V., POMA, O. and ALOMÍA, M. 2004. Fossil whale preservation implies high diatom accumulation rate in the Miocene–Pliocene Pisco Formation of Peru. *Geology*, **32**, 165-168.

BROWNELL, R. L., JR 1989. Franciscana *Pontoporia blainvillei* (Gervais and d'Orbigny, 1844). 45-67. *In* RIDGWAY, S. H. and HARRISON, R. (eds). *Handbook of marine mammals, vol. 4: River dolphins and the larger toothed whales*. Academic Press, London.

CASSENS, I., VICARIO, S., WADDELL, V. G., BALCHOWSKY, H., VAN BELLE, D., DING, W., CHEN, F., MOHAN, R. S. L., SIMOES-LOPES, P. C., BASTIDA, R., MEYER, A., STANHOPE, M. J. and MILINKOVITCH, M. C. 2000. Independent adaptation to riverine habitats allowed survival of ancient cetacean lineages. *Proceedings of the National Academy of Sciences*, **97**, 11343-11347.

CHEN, P. 1989. Baiji *Lipotes vexillifer* Miller, 1918. 25-43. *In* RIDGWAY, S. H. and HARRISON, R. (eds). *Handbook of marine mammals, vol. 4: River dolphins and the larger toothed whales*. Academic Press, London.

COLLARETA, A., LANDINI, W., LAMBERT, O., POST, K., TINELLI, C., DI CELMA, C., PANETTA, D., TRIPODI, M., SALVADORI, P., CARAMELLA, D., MARCHI, D., URBINA, M. and BIANUCCI, G. 2015. Piscivory in a Miocene Cetotheriidae of Peru: first record of fossilized stomach content for an extinct baleen-bearing whale. *The Science of Nature*, **102**, 1-12.

COZZUOL, M. 2010. Fossil record and evolutionary history of Inioidea. 193-217. *In* RUIZ-GARCIA, M. and SHOSTELL, J. (eds). *Biology, evolution and conservation of river dolphins within South America and Asia*. Nova Science Publishers, New York.

DEVRIES, T. J. 1998. Oligocene deposition and Cenozoic sequence boundaries in the Pisco Basin (Peru). *Journal of South American Earth Sciences*, **11**, 217-231.

DEVRIES, T. and JUD, N. 2018. Lithofacies patterns and paleogeography of the Miocene Chilcatay and lower Pisco depositional sequences (East Pisco Basin, Peru). *Boletín de la Sociedad Geológica del Perú*, **8**, 124-167.

DEVRIES, T. and SCHRADER, H. 1997. Middle Miocene marine sediments in the Pisco basin (Peru). *Boletín de la Sociedad Geológica del Perú*, **87**, 1-13.

DI CELMA, C., MALINVERNO, E., GARIBOLDI, K., GIONCADA, A., RUSTICHELLI, A., PIERANTONI, P., LANDINI, W., BOSIO, G., TINELLI, C. and BIANUCCI, G. 2016. Stratigraphic framework of the late Miocene to Pliocene Pisco Formation at Cerro Colorado (Ica Desert, Peru). *Journal of Maps*, **12**, 515-529.

DI CELMA, C., MALINVERNO, E., BOSIO, G., COLLARETA, A., GARIBOLDI, K., GIONCADA, A., MOLLI, G., BASSO, D., VARAS-MALCA, R. M., PIERANTONI, P. P., VILLA, I. M., LAMBERT, O., LANDINI, W., SARTI, G., CANTALAMESSA, G., URBINA, M. and BIANUCCI, G. 2017. Sequence stratigraphy and paleontology of the upper Miocene Pisco Formation along the western side of the lower Ica Valley (Ica desert, Peru) *Rivista Italiana di Paleontologia e Stratigrafia* **123**, 255-273.

DI CELMA, C., MALINVERNO, E., BOSIO, G., GARIBOLDI, K., COLLARETA, A., GIONCADA, A., LANDINI, W., PIERANTONI, P. P. and BIANUCCI, G. 2018. Intraformational unconformities as a record of late Miocene eustatic falls of sea level in the Pisco Formation (southern Peru). *Journal of Maps*, **14**, 607-619.

DUNBAR, R. B., MARTY, R. C. and BAKER, P. A. 1990. Cenozoic marine sedimentation in the Sechura and Pisco basins, Peru. *Palaeogeography, Palaeoclimatology, Palaeoecology* **77**, 235-261.

EHRET, D. J., MCFADDEN, B. J., JONES, D. S., DEVRIES, T. J., FOSTER, D. A. and SALAS-GISMONDI, R. 2012. Origin of the white shark *Carcharodon* (Lamniformes: Lamnidae) based on recalibration of the Upper Neogene Pisco Formation of Peru. *Palaeontology*, **55**, 1139-1153.

FLOWER, W. H. 1867. Description of the skeleton of *Inia geoffrensis* and the skull of *Pontoporia blainvillii*, with remarks on the systematic position of these animals in the Order Cetacea. *Transactions of the Zoological Society of London*, **6**, 87-116.

FRAINER, G., HUGGENBERGER, S. and MORENO, I. B. 2015. Postnatal development of franciscana's (*Pontoporia blainvillei*) biosonar relevant structures with potential implications for function, life history, and bycatch. *Marine Mammal Science*, **31**, 1193-1212.

FRASER, F. C. and PURVES, P. E. 1960. Hearing in cetaceans: Evolution of the accessory air sacs and the structure of the outer and middle ear in recent cetaceans. *Bulletin of the British Museum (Natural History), Zoology*, **7**, 1-140.

GALATIUS, A. and KINZE, C. C. 2003. Ankylosis patterns in the postcranial skeleton and hyoid bones of the harbour porpoise (*Phocoena phocoena*) in the Baltic and North Sea. *Canadian Journal of Zoology* **81**, 1851-1861.

GARIBOLDI, K., BOSIO, G., MALINVERNO, E., GIONCADA, A., DI CELMA, C., VILLA, I. M., URBINA, M. and BIANUCCI, G. 2017. Biostratigraphy, geochronology and sedimentation rates of the upper Miocene Pisco Formation at two important marine vertebrate fossil-bearing sites of southern Peru. *Newsletters on Stratigraphy*, **50**, 417-444.

GEISLER, J. H., MCGOWEN, M. R., YANG, G. and GATESY, J. 2011. A supermatrix analysis of genomic, morphological, and paleontological data for crown Cetacea. *BMC Evolutionary Biology* **11**, 1-22.

GEISLER, J. H., GODFREY, S. J. and LAMBERT, O. 2012. A new genus and species of late Miocene inioid (Cetacea: Odontoceti) from the Meherrin River, North Carolina, U.S.A. *Journal of Vertebrate Paleontology*, **32**, 198-211.

GIBSON, M. L. and GEISLER, J. H. 2009. A new Pliocene dolphin (Cetacea: Pontoporiidae), from the Lee Creek Mine, North Carolina. *Journal of Vertebrate Paleontology*, **29**, 966-971.

GIONCADA, A., COLLARETA, A., GARIBOLDI, K., LAMBERT, O., DI CELMA, C., BONACCORSI, E., URBINA, M. and BIANUCCI, G. 2016. Inside baleen: Exceptional microstructure preservation in a late Miocene whale skeleton from Peru. *Geology*, **44**, 839-842.

GIONCADA, A., GARIBOLDI, K., COLLARETA, A., DI CELMA, C., BOSIO, G., MALINVERNO, E., LAMBERT, O., PIKE, J., URBINA, M. and BIANUCCI, G. 2018. Looking for the key to preservation of fossil marine vertebrates in the Pisco Formation of Peru: new insights from a small dolphin skeleton. *Andean Geology*, **45**, 379-398.

GODFREY, S. J. and BARNES, L. G. 2008. A new genus and species of late Miocene pontoporiid dolphin (Cetacea: Odontoceti) from the St. Marys Formation in Maryland. *Journal of Vertebrate Paleontology*, **28**, 520-528.

GUTSTEIN, C. S., COZZUOL, M. A., VARGAS, A. O., SUÁREZ, M. E., SCHULTZ, C. L., & RUBILAR-ROGERS, D. 2009. Patterns of skull variation of *Brachydelphis* (Cetacea, Odontoceti) from the Neogene of the southeastern Pacific. *Journal of Mammalogy*, **90**, 504-519.

GUTSTEIN, C. S., COZZUOL, M. A. and PYENSON, N. D. 2014. The antiquity of riverine adaptations in Iniidae (Cetacea, Odontoceti) documented by a humerus from the Late Miocene of the Ituzaingó Formation, Argentina. *The Anatomical Record*, **297**, 1096-1102.

HAMILTON, H., CABALLERO, S., COLLINS, A. G. and BROWNELL, R. L., JR 2001. Evolution of river dolphins. *Proceedings of the Royal Society of London (B)*, **268**, 549-556.

HAMPEL, A., KUKOWSKI, N., BIALAS, J., HUEBSCHER, C. and HEINBOCKEL, R. 2004. Ridge subduction at an erosive margin: The collision zone of the Nazca Ridge in southern Peru. *Journal of Geophysical Research: Solid Earth*, **109**, article #B02101.

HSU, J. T. 1992. Quaternary uplift of the Peruvian coast related to the subduction of the Nazca Ridge: 13.5 to 15.6 degrees south latitude. *Quaternary International*, **15**, 87-97.

HUGGENBERGER, S., VOGL, T. J. and OELSCHLÄGER, H. H. 2010. Epicranial complex of the La Plata dolphin (*Pontoporia blainvillei*): Topographical and functional implications. *Marine mammal science*, **26**, 471-481.

LAMBERT, O., BIANUCCI, G. and POST, K. 2009. A new beaked whale (Odontoceti, Ziphiidae) from the middle Miocene of Peru. *Journal of Vertebrate Paleontology*, **29**, 910-922.

LAMBERT, O., BIANUCCI, G., POST, K., MUIZON, C., DE, SALAS-GISMONDI, R., URBINA, M. and REUMER, J. 2010. The giant bite of a new raptorial sperm whale from the Miocene epoch of Peru. *Nature*, **466**, 105-108.

LAMBERT, O. and MUIZON, C., DE 2013. A new long-snouted species of the Miocene pontoporiid dolphin *Brachydelphis* and a review of the Mio-Pliocene marine mammal levels in the Sacaco Basin, Peru. *Journal of Vertebrate Paleontology*, **33**, 709-721.

LAMBERT, O., COLLARETA, A., LANDINI, W., POST, K., RAMASSAMY, B., DI CELMA, C., URBINA, M. and BIANUCCI, G. 2015. No deep diving: evidence of

predation on epipelagic fish for a stem beaked whale from the Late Miocene of Peru. *Proceedings of the Royal Society B*, **282**, 20151530.

LAMBERT, O., BIANUCCI, G., URBINA, M. and GEISLER, J. H. 2017. A new inioid (Cetacea, Odontoceti, Delphinida) from the Miocene of Peru and the origin of modern dolphin and porpoise families. *Zoological Journal of the Linnean Society*, **179**, 919-946.

LAMBERT, O., AUCLAIR, C., CAUXEIRO, C., LOPEZ, M. and ADNET, S. 2018. A close relative of the Amazon river dolphin in marine deposits: a new Iniidae from the late Miocene of Angola. *PeerJ*, **6**, e5556.

LANDINI, W., COLLARETA, A., DI CELMA, C., MALINVERNO, E., URBINA, M. and BIANUCCI, G. 2019. The early Miocene elasmobranch assemblage from Zamaca (Chilcatay Formation, Peru). *Journal of South American Earth Sciences*, **91**, 352-371.

LANDINI, W., COLLARETA, A., PESCI, F., DI CELMA, C., URBINA, M. and BIANUCCI, G. 2017. A secondary nursery area for the copper shark *Carcharhinus brachyurus* from the late Miocene of Peru. *Journal of South American Earth Sciences*, **78**, 164-174.

LEÓN, W., ALEMAN, A., TORRES, V., ROSELL, W. and DE LA CRUZ, O. 2008. Estratigrafía, sedimentología y evolución tectónica de la cuenca Pisco Oriental. *Boletín INGEMMET*, **27**, 1-144.

MACHARÉ, J. and ORTLIEB, L. 1992. Plio-Quaternary vertical motions and the subduction of the Nazca Ridge, central coast of Peru. *Tectonophysics*, **205**, 97-108.

MAROCCO, R. and MUIZON, C. DE. 1988. Le Bassin Pisco, bassin cénozoïque d'avant arc de la côte du Pérou central: Analyse géodynamique de son remplissage. *Géodynamique*, **3**, 3-19.

MARX, F. G., LAMBERT, O. and UHEN, M. D. 2016. Topics in Paleobiology. *Cetacean paleobiology*. John Wiley & Sons, Chichester, UK, 319 pp.

MCCURRY, M. R. and PYENSON, N. D. 2018. Hyper-longirostry and kinematic disparity in extinct toothed whales. *Paleobiology*, **45**, 21-29.

MCGOWEN, M. R., TSAGKOGEORGA, G., ÁLVAREZ-CARRETERO, S., DOS REIS, M., STRUEBIG, M., DEAVILLE, R., JEPSON, P. D., JARMAN, S., POLANOWSKI, A. and MORIN, P. A. 2019. Phylogenomic resolution of the cetacean tree of life using target sequence capture. *Systematic biology*.

MEAD, J. G. and FORDYCE, R. E. 2009. The therian skull: a lexicon with emphasis on the odontocetes. *Smithsonian Contributions to Zoology*, **627**, 1-248.

MILLER, G. S., JR. 1918. A new river-dolphin from China. *Smithsonian Miscellaneous Collections*, **68**, 1-12.

MORAN, M. M., BAJPAI, S., GEORGE, J. C., SUYDAM, R., USIP, S. and THEWISSEN, J. G. M. 2015. Intervertebral and epiphyseal fusion in the postnatal ontogeny of cetaceans and terrestrial mammals. *Journal of Mammalian Evolution*, **22**, 93-109.

MUIZON, C., DE 1984. Les vertébrés de la Formation Pisco (Pérou). Deuxième partie: Les Odontocètes (Cetacea, Mammalia) du Pliocène inférieur de Sud-Sacaco. *Travaux de l'Institut Français d'Etudes Andines* **27**, 1-188.

MUIZON, C., DE 1988*a*. Les vertébrés fossiles de la Formation Pisco (Pérou). Troisième partie: Les Odontocètes (Cetacea, Mammalia) du Miocène. *Travaux de l'Institut Français d'Etudes Andines*, **42**, 1-244.

MUIZON, C., DE 1988*b*. Les relations phylogénétiques des Delphinida. *Annales de Paléontologie*, **74**, 159-227.

MURAKAMI, M. 2016. A new extinct inioid (Cetacea, Odontoceti) from the Upper Miocene Senhata Formation, Chiba, central Japan: the first record of Inioidea from the North Pacific Ocean. *Paleontological Research*, **20**, 207-225.

PARHAM, J. F. and PYENSON, N. D. 2010. New sea turtle from the Miocene of Peru and the iterative evolution of feeding ecomorphologies since the Cretaceous. *Journal of Paleontology*, **84**, 231-247.

PEREDO, C. M., UHEN, M. D. and NELSON, M. D. 2018. A new kentriodontid (Cetacea: Odontoceti) from the early Miocene Astoria Formation and a revision of the stem delphinidan family Kentriodontidae. *Journal of Vertebrate Paleontology*, e1411357.

PILGER, R. H., JR 1981. Plate reconstructions, aseismic ridges, and low-angle subduction beneath the Andes. *Geological Society of America Bulletin*, **92**, 448-456.

PILLERI, G. and GIHR, M. 1969. Zur anatomie und pathologie von *Inia geoffrensis* de Blainville 1817 (Cetacea, Susuidae) aus dem Beni, Bolivien. *Investigations on Cetacea*, **1**, 94-106.

POST, K., LOUWYE, S. and LAMBERT, O. 2017. *Scaldiporia vandokkumi*, a new pontoporiid (Mammalia, Cetacea, Odontoceti) from the Late Miocene to earliest Pliocene of the Westerschelde estuary (The Netherlands). *PeerJ*, **5**, e3991.

PYENSON, N. D. and HOCH, E. 2007. Tortonian pontoporiid odontocetes from the Eastern North Sea. *Journal of Vertebrate Paleontology*, **27**, 757-762.

PYENSON, N. D. and SPONBERG, S. N. 2011. Reconstructing body size in extinct crown Cetacea (Neoceti) using allometry, phylogenetic methods and tests from the fossil record. *Journal of Mammalian Evolution*, **18**, 269-288.

PYENSON, N. D., VÉLEZ-JUARBE, J., GUTSTEIN, C. S., LITTLE, H., VIGIL, D. and O'DEA, A. 2015. *Isthminia panamensis*, a new fossil inioid (Mammalia, Cetacea) from the Chagres Formation of Panama and the evolution of 'river dolphins' in the Americas. *PeerJ*, **3**, e1227.

RAMASSAMY, B., LAMBERT, O., COLLARETA, A., URBINA, M. and BIANUCCI, G. 2018. Description of the skeleton of the fossil beaked whale *Messapicetus gregarius*: searching potential proxies for deep-diving abilities. *Fossil Record*, **21**, 11-32.

SEAGARS, D. J. 1982. Jaw structure and functional mechanics of six delphinids (Cetacea: Odontoceti). Unpublished master thesis, San Diego State University, 179 pp.

STUCCHI, M., VARAS-MALCA, R. M. and URBINA-SCHMITT, M. 2016. New Miocene sulid birds from Peru and considerations on their Neogene fossil record in the Eastern Pacific Ocean. *Acta Palaeontologica Polonica*, **61**, 417-427.

SUESS, E., VON HUENE, R. and EMEIS, K. 1988. Introduction, objectives, and principal results, Leg 112, Peru continental margin. *Proceedings of ODP, Initial Reports*, **112**, 5-23.

SWOFFORD, D. L. 2003. *PAUP*. Phylogenetic analysis using parsimony (*and other methods). Version 4*. Sinauer Associates, Sunderland, Massachusetts.

THORNBURG, T. M. and KULM, L. D. 1981. Sedimentary basins of the Peru continental margin: Structure, stratigraphy, and Cenozoic tectonics from 6°S to 16°S latitude. *In* KULM, L.D., DYMOND, J., DASCH, E.J., and HUSSONG, D.M. (eds). *Nazca plate: crustal formation and Andean convergence*. *Geological Society of America Memoir*, **154**, 393-422.

TRAVIS, R. B., GONZALES, G. and PARDO, A. 1976. Hydrocarbon Potential of Coastal Basins of Peru. *AAPG Memoir*, **25**, 331-338.

VAN BENEDEN, P.-J. and GERVAIS, P. 1880. *Ostéographie des cétacés vivants et fossiles*. Arthus Bertrand, Paris, 634 pp.

WERTH, A. J. 2006. Mandibular and dental variation and the evolution of suction feeding in Odontoceti. *Journal of Mammalogy*, **87**, 579-588.

TABLE CAPTIONS

TABLE 1. Measurements (in millimetres) on the six crania of *Samaydelphis chacaltanae* described in this work. +, incomplete; e, estimate; -, not preserved.

TABLE 2. Measurements (in millimetres) on the axis and one thoracic vertebra found associated to the cranium of *Samaydelphis chacaltanae* MUSUM 565. +, incomplete.

FIGURE CAPTIONS

FIG. 1. A. Sketch map of the major structural trends and basins of coastal Peru. The red dashed rectangle indicates the location of the East Pisco Basin, shown in detail in panel B. Redrawn and modified from Travis *et al.* (1976) and Thornburg & Kulm (1981). **B.** Schematic geological map of the East Pisco Basin, showing the areas of outcrop of the Cenozoic basin fill and the location of the sites (black stars) where the holotype and referred specimens of the new inioid taxon *Samaydelphis chacaltanae* described herein were found (CC = Cerro Colorado; CV = Corre Viento; CLB = Cerro la Bruja; ZAN = Cerros Cadena de los Zanjones). Redrawn and modified from DeVries & Schrader (1997).
Planned for page width.

FIG. 2. Stratigraphic sections of several localities of the East Pisco Basin showing the distribution in late Miocene layers of the Pisco Formation of fossil inioids including the holotype of *Samaydelphis chacaltanae* MUSM 566. Combined absolute ($^{40}Ar/^{39}Ar$ on ash layers) and biostratigraphical (diatoms) datings (Gariboldi *et al.* 2019; Bosio *et al.* 2019,

2020b) constraining the age of the fossil inioids are also reported along the sections, together with the position of the main marker beds (Di Celma *et al.* 2016, 2018).

Planned for page width.

FIG. 3. Cranium of *Samaydelphis chacaltanae* MUSM 566 (holotype) in dorsal (A, B) and right lateral (C) views.

Planned for page width.

FIG. 4. Cranium of *Samaydelphis chacaltanae* MUSM 566 (holotype) in ventral (A), anterodorsal (B), and posterior (C) views.

Planned for page width.

FIG. 5. Cranium of *Samaydelphis chacaltanae* MUSM 565 in dorsal (A), left lateral (B), ventral (C), posterior (D), and anterodorsal (E) views.

Planned for page width.

FIG. 6. Partial cranium (facial region) of *Samaydelphis chacaltanae* MUSM 2541 (A) and vertex of MUSM 2512 (B) in dorsal view.

Planned for page width.

FIG. 7. Cranium of *Samaydelphis chacaltanae* MUSM 3903 in dorsal and right lateral view and skull of MUSM 3902 in right lateral view.

Planned for page width.

FIG. 8. Fragment of right mandible of *Samaydelphis chacaltanae* MUSM 2541 in lateral view and detached posterior lower tooth of MUSM 2541 in mesial/distal view.
Planned for half page width.

FIG. 9. Vertebrae of *Samaydelphis chacaltanae* MUSM 565. A-C, atlas in anterior, posterior (B), and ventral (C) views. D-E, thoracic vertebra in posterior (D) and ventral (E) views.
Planned for page width.

FIG. 10. Phylogenetic relationships of *Samaydelphis chacaltanae* with other inioids. Delphinidan part of the single most parsimonious tree resulting from the heuristic search based on a morphological character-taxon matrix, with a molecular constraint on extant cetacean species applied as a backbone (based on McGowen *et al.* 2019). The clade Delphinoidea is collapsed for clarity (see Supplementary File 3 for the complete tree). Taxa in bold correspond to inioids from the late Neogene of the Pisco Basin, Peru. Pontop. for Pontoporiidae; Rec. for Recent species; sub-Rec. for the recently extinct *Lipotes vexillifer*. Number below nodes correspond to bootstrap values (only the ones > 50 provided).
Planned for half page width.

FIG. 11. Comparison of rostral proportions in extinct and extant inioids. Graph showing the range of the rostrum length (rl)/bizygomatic width (bzw) ratio in a series of inioids from the Pisco Formation and the extant *Pontoporia blainvillei* and *Inia* spp. Numbers above ranges correspond to the number of specimens measured. Taxa that have been recorded from the stratal package P1 of the Pisco Formation are circled. Measurements taken from Flower (1867), Pilleri & Gihr (1969), Muizon (1984), Lambert & Muizon (2013), and Lambert *et al.* (2017). Schematic reconstructions of crania in dorsal view for late Miocene inioids from the

Pisco Formation. Drawings of *Brachydelphis* spp. and *Brujadelphis ankylorostris* modified from Lambert & Muizon (2013) and Lambert *et al.* (2017), respectively. All crania scaled at the same bizygomatic width.

Planned for page width.

	MUSM 566 (holotype)	**MUSM 565**	**MUSM 2541**	**MUSM 2512**	**MUSM 3902**	**MUSM 3903**
Condylobasal length	+295 (e310)	+310 (e320)	-	-	-	+310 (e320)
Rostrum length	+165 (e180)	+170 (e180)	-	-	165	+175 (e185)
Width of the rostrum at its base	75	68.5	-	-	e64	e70
Width of premaxillae at rostrum base	44.5	42	-	-	e42	42
Preorbital width of the skull	113	111	-	-	-	e110
Postorbital width of the skull	+132	133	-	-	-	++125
Distance between premaxillary foramina	24	21.5	24.5	-	21	22
Maximum width of bony nares	27	25	29	-	24	28
Anteroposterior length of bony nares	24.5	23.5	28	-	26	e28
Maximum width of premaxillary sac fossae	52	51	59	-	50	53
Maximum width of premaxillae	62	62	e66	-	55	62
Maximum width of nasals	23	27	27.5	26	25	27
Maximum length of nasals	32	31.5	37	29.5	-	31.5
Minimum distance between maxillae across vertex	17.5	18	15.5	11	14	15
Bizygomatic width	148	152	-	-	-	144
Maximum width of exoccipitals	118	120	-	-	-	115
Width of occipital condyles	59	59	-	-	-	57
Maximum width of foramen magnum	27.5	26.5	-	-	-	27
Height of foramen magnum	25	24	-	-	-	24
Orbit length	36.5	e37	-	-	-	-
Length of right temporal fossa	79	83	-	-	79	81
Height of right temporal fossa	53	60	-	-	57	54
Length of a segment of 8 dental alveoli (maxilla)	40	-	-	-	37	41
Length of a segment of 8 dental alveoli (mandible)	-	-	41	-	-	-

Axis	
Maximum width across anterior articular surfaces	51.1
Width across transverse processes	72.8
Width of neural arch	+20
Width of posterior articular surface	24.5
Height of posterior articular surface	18.6
Thoracic	
Anterior width of centrum	25.5
Anterior height of centrum	22.1
Posterior width of centrum	27.4
Posterior height of centrum	30.2
Length of the centrum	33.1
Width across transverse processes	74.5
Width of neural canal	14.4
Height of neural spine	+41.4

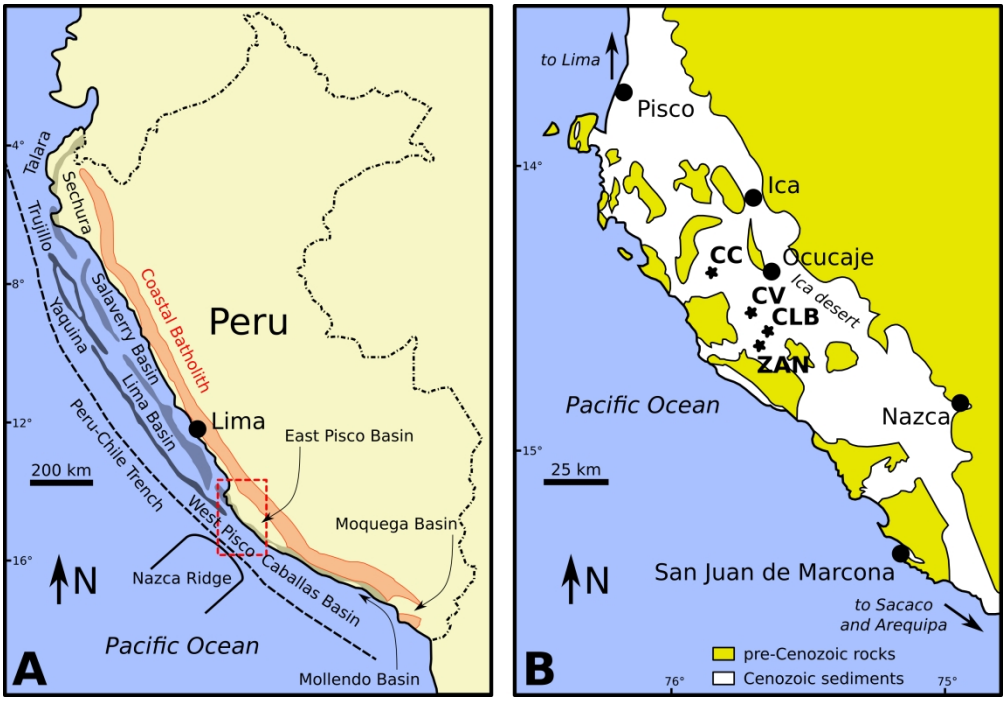

FIG. 1. A. Sketch map of the major structural trends and basins of coastal Peru. The red dashed rectangle indicates the location of the East Pisco Basin, shown in detail in panel B. Redrawn and modified from Travis et al. (1976) and Thornburg & Kulm (1981). B. Schematic geological map of the East Pisco Basin, showing the areas of outcrop of the Cenozoic basin fill and the location of the sites (black stars) where the holotype and referred specimens of the new inioid taxon Samaydelphis chacaltanae described herein were found (CC = Cerro Colorado; CV = Corre Viento; CLB = Cerro la Bruja; ZAN = Cerros Cadena de los Zanjones). Redrawn and modified from DeVries & Schrader (1997).
Planned for page width.

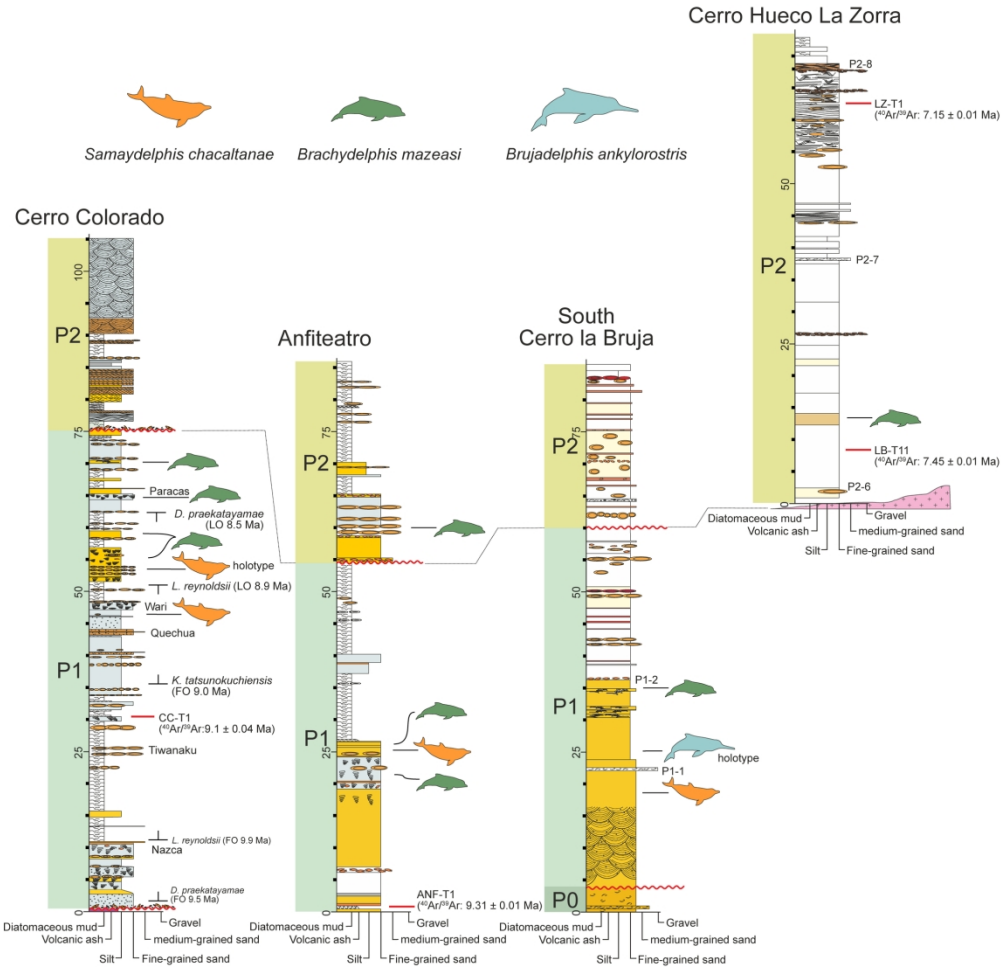

FIG. 2. Stratigraphic sections of several localities of the East Pisco Basin showing the distribution in late Miocene layers of the Pisco Formation of fossil inioids including the holotype of Samaydelphis chacaltanae MUSM 566. Combined absolute (40Ar/39Ar on ash layers) and biostratigraphical (diatoms) datings (Gariboldi et al. 2019; Bosio et al. 2019, 2020b) constraining the age of the fossil inioids are also reported along the sections, together with the position of the main marker beds (Di Celma et al. 2016, 2018).
Planned for page width.

193x186mm (300 x 300 DPI)

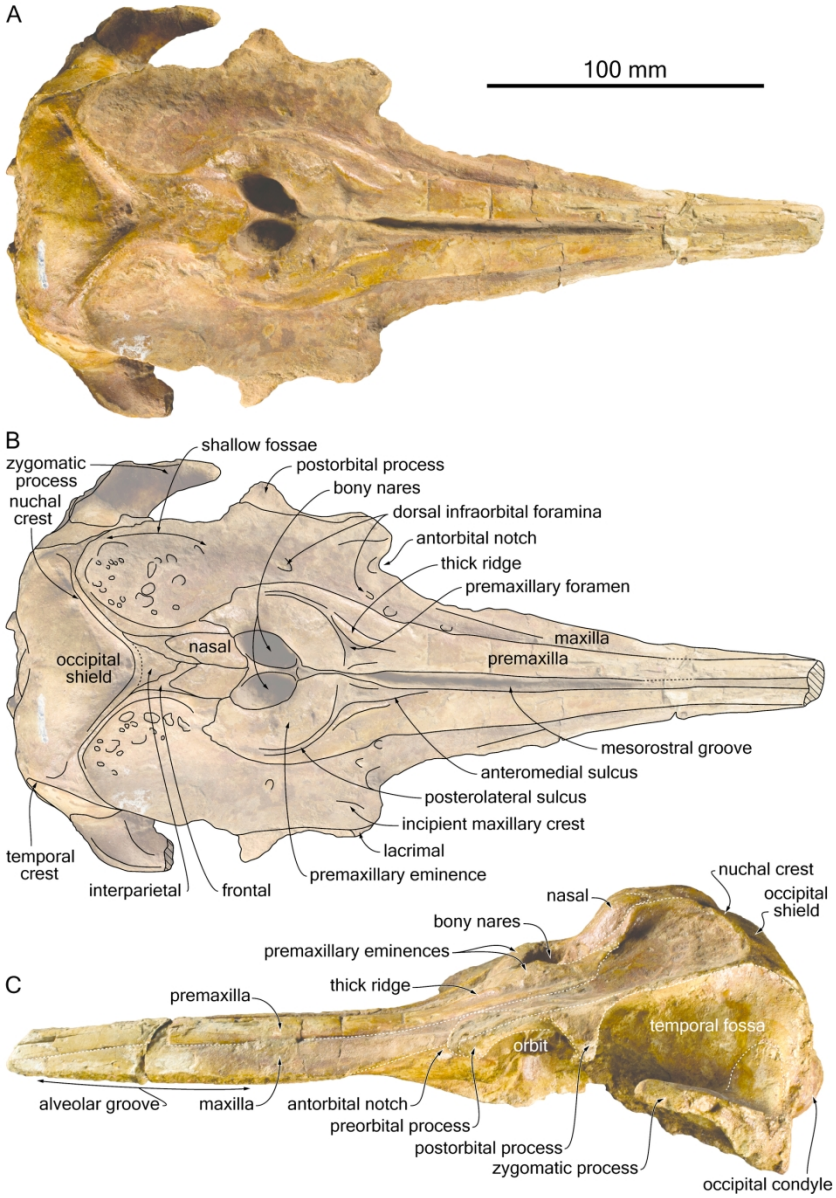

FIG. 3. Cranium of Samaydelphis chacaltanae MUSM 566 (holotype) in dorsal (A, B) and right lateral (C) views.
Planned for page width.

150x215mm (300 x 300 DPI)

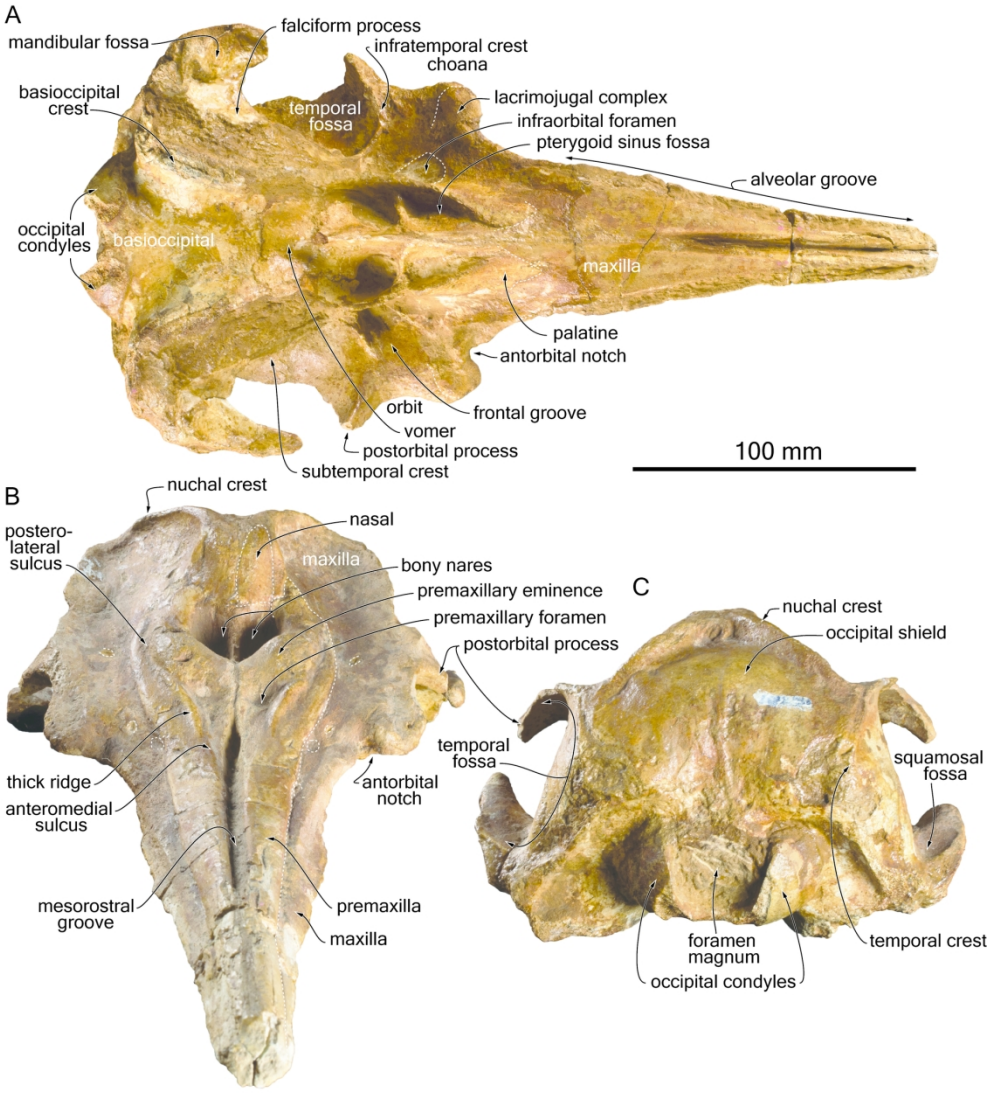

FIG. 4. Cranium of Samaydelphis chacaltanae MUSM 566 (holotype) in ventral (A), anterodorsal (B), and posterior (C) views.
Planned for page width.

171x190mm (300 x 300 DPI)

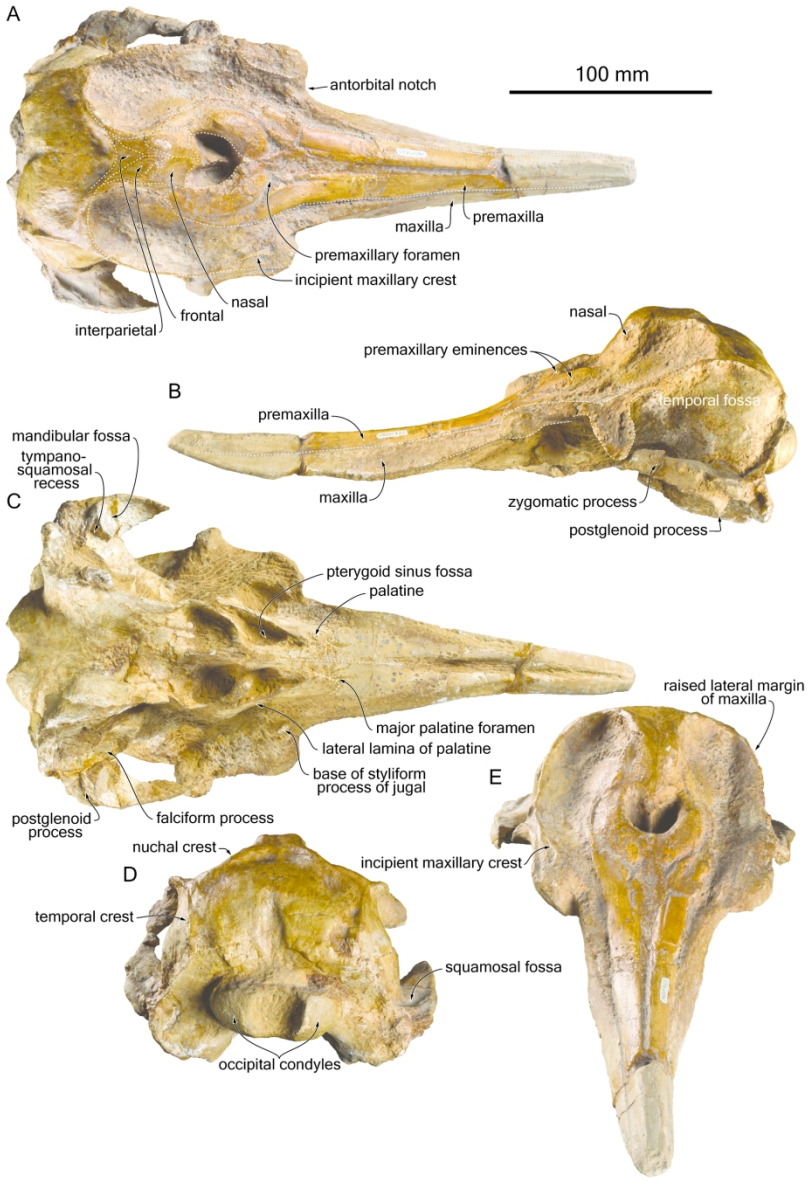

FIG. 5. Cranium of Samaydelphis chacaltanae MUSM 565 in dorsal (A), left lateral (B), ventral (C), posterior (D), and anterodorsal (E) views.
Planned for page width.

167x244mm (300 x 300 DPI)

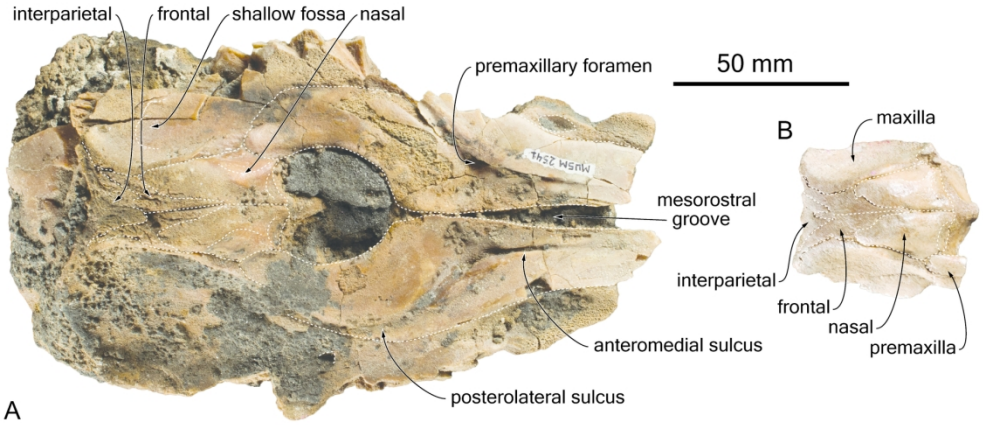

FIG. 6. Partial cranium (facial region) of Samaydelphis chacaltanae MUSM 2541 (A) and vertex of MUSM 2512 (B) in dorsal view.
Planned for page width.

167x77mm (300 x 300 DPI)

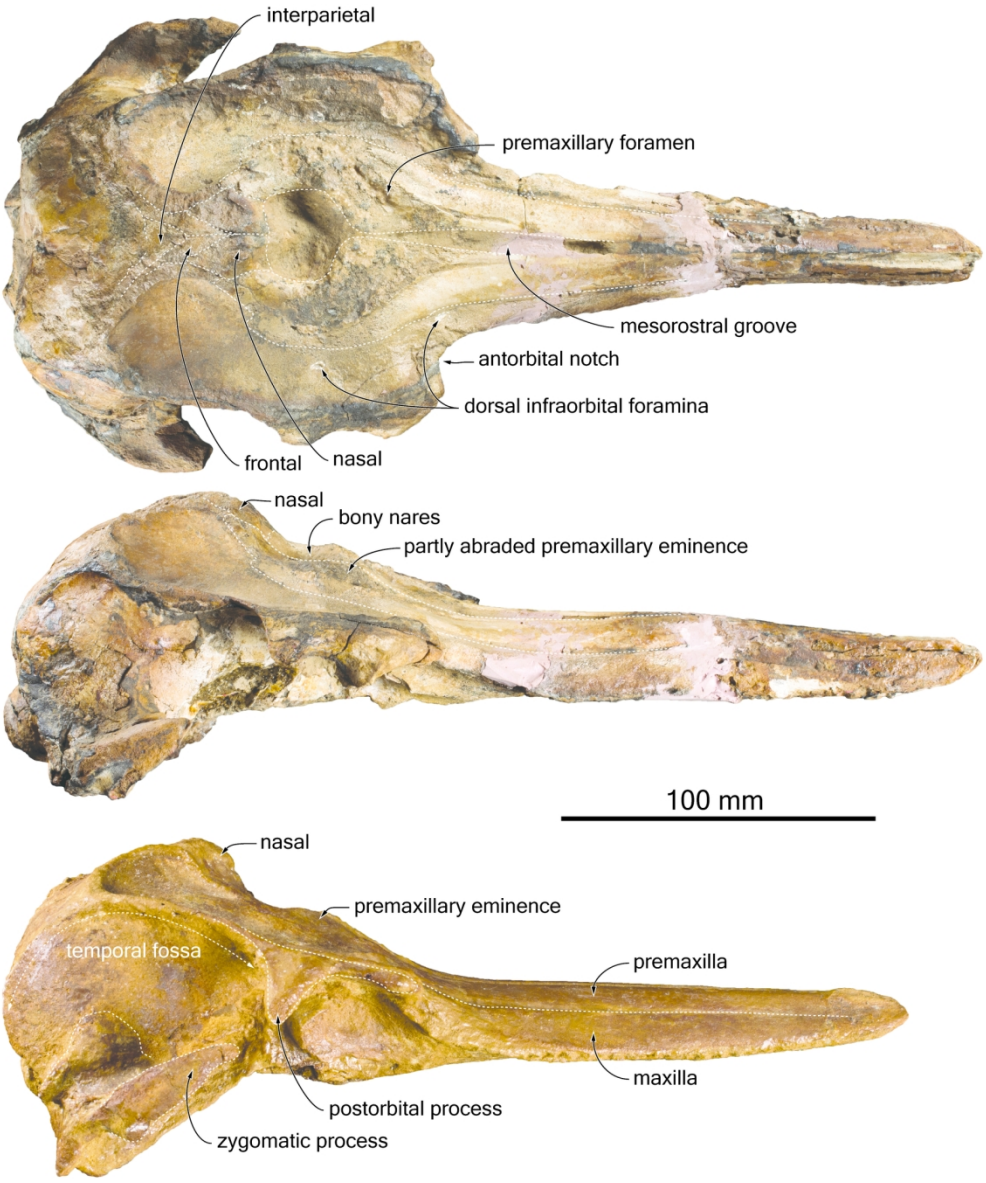

FIG. 7. Cranium of Samaydelphis chacaltanae MUSM 3903 in dorsal and right lateral view and skull of MUSM 3902 in right lateral view.
Planned for page width.

153x181mm (300 x 300 DPI)

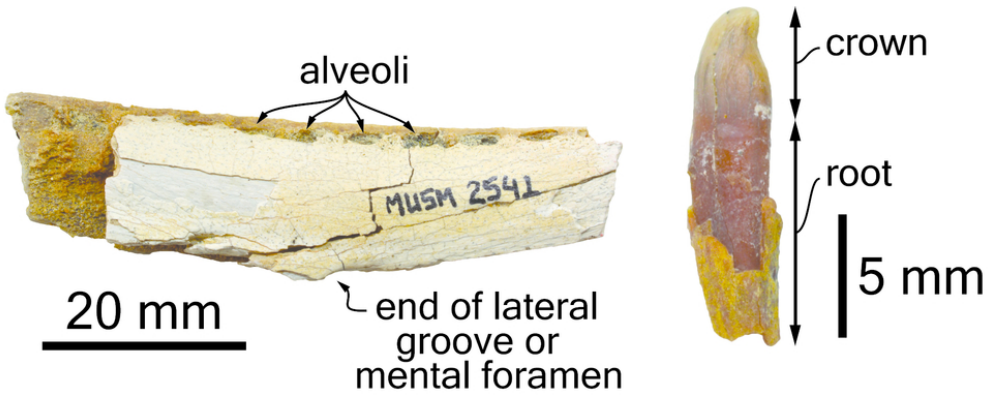

FIG. 8. Fragment of right mandible of Samaydelphis chacaltanae MUSM 2541 in lateral view and detached posterior lower tooth of MUSM 2541 in mesial/distal view.
Planned for half page width.

81x32mm (300 x 300 DPI)

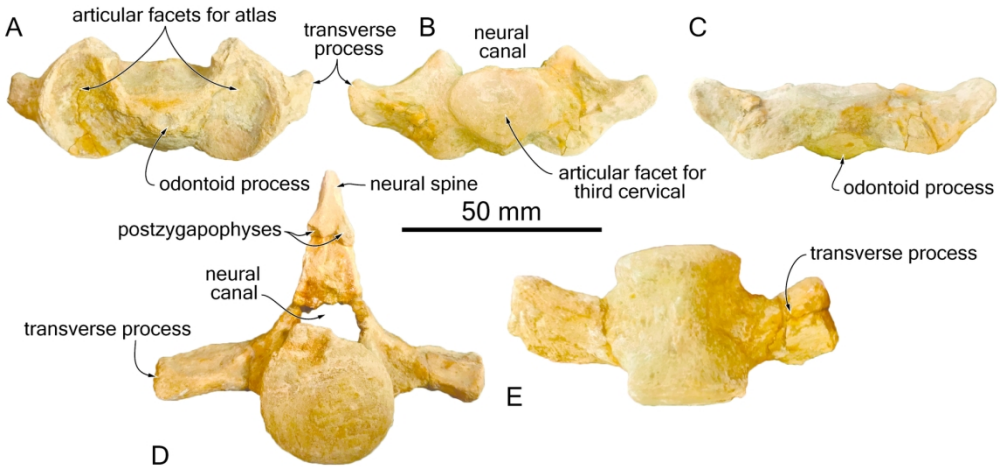

FIG. 9. Vertebrae of Samaydelphis chacaltanae MUSM 565. A-C, atlas in anterior, posterior (B), and ventral (C) views. D-E, thoracic vertebra in posterior (D) and ventral (E) views.
Planned for page width.

160x81mm (300 x 300 DPI)

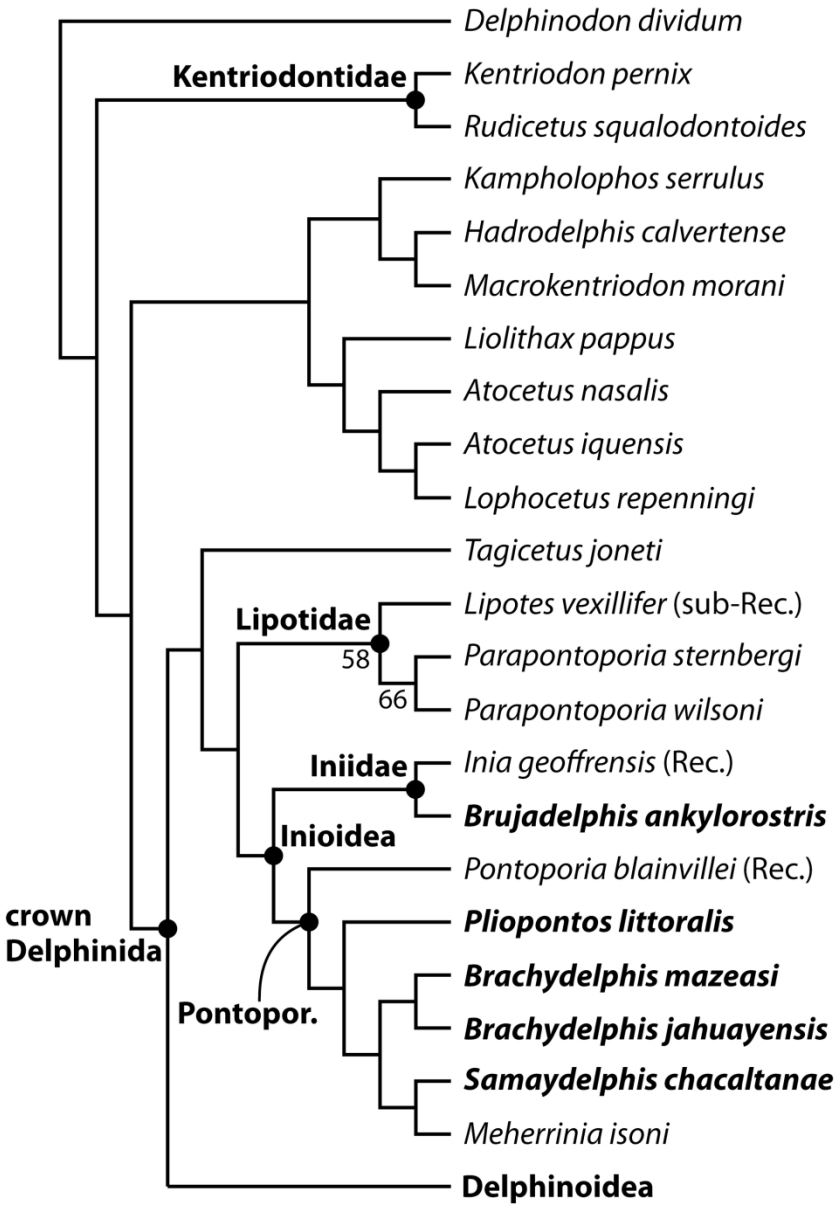

FIG. 10. Phylogenetic relationships of Samaydelphis chacaltanae with other inioids. Delphinidan part of the single most parsimonious tree resulting from the heuristic search based on a morphological character-taxon matrix, with a molecular constraint on extant cetacean species applied as a backbone (based on McGowen et al. 2019). The clade Delphinoidea is collapsed for clarity (see Supplementary File 3 for the complete tree). Taxa in bold correspond to inioids from the late Neogene of the Pisco Basin, Peru. Pontop. for Pontoporiidae; Rec. for Recent species; sub-Rec. for the recently extinct Lipotes vexillifer. Number below nodes correspond to bootstrap values (only the ones > 50 provided).
Planned for half page width.

82x119mm (600 x 600 DPI)

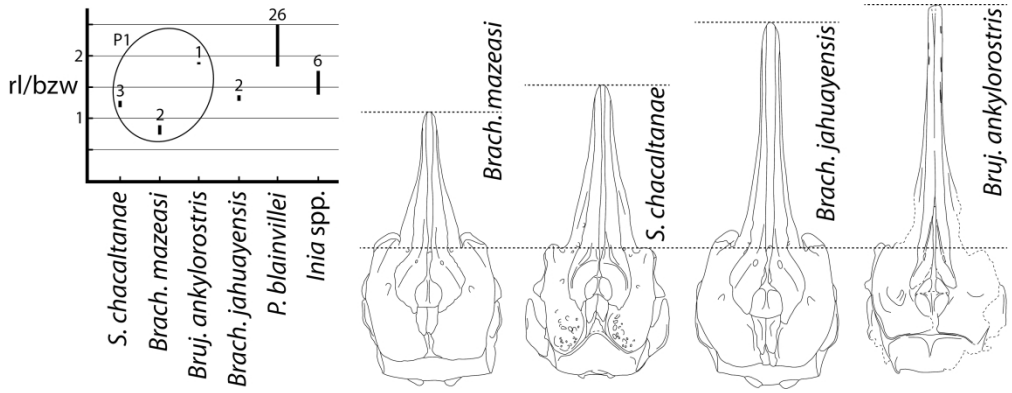

FIG. 11. Comparison of rostral proportions in extinct and extant inioids. Graph showing the range of the rostrum length (rl)/bizygomatic width (bzw) ratio in a series of inioids from the Pisco Formation and the extant Pontoporia blainvillei and Inia spp. Numbers above ranges correspond to the number of specimens measured. Taxa that have been recorded from the stratal package P1 of the Pisco Formation are circled. Measurements taken from Flower (1867), Pilleri & Gihr (1969), Muizon (1984), Lambert & Muizon (2013), and Lambert et al. (2017). Schematic reconstructions of crania in dorsal view for late Miocene inioids from the Pisco Formation. Drawings of Brachydelphis spp. and Brujadelphis ankylorostris modified from Lambert & Muizon (2013) and Lambert et al. (2017), respectively. All crania scaled at the same bizygomatic width. Planned for page width.

160x61mm (600 x 600 DPI)

Strict consensus tree